Earth and Planetary Science
https://journals.nasspublishing.com/index.php/eps

ARTICLE

Cosmic Ray Modulation Across Solar Cycles 23 and 24: Phase Dependent Variability and Geomagnetic Storm Effects

Chika Onuchukwu * , ***Edwin Dio***

Industrial Physics, Chukwuemeka Odumegwu Ojukwu University, 54 Egbu Road, Uli Campus, Awka 420102, Anambra, Nigeria

ABSTRACT

This study investigates the modulation of cosmic ray (CR) intensity in response to solar and heliospheric variability across the ascending (ASC) and descending (DSC) phases of Solar Cycles (SCs) 23 and 24. Using daily-averaged data, we analyze sunspot number (SSN) as a proxy for solar activity, solar wind parameters - interplanetary magnetic field (IMF), solar wind plasma density (SWPD), speed (SWS), temperature (SWT) - and geomagnetic indices (Kp, Dst, ap). Geomagnetic storms were categorized by intensity based on Dst index thresholds. Distribution analyses reveal broadly consistent trends for SSN, IMF, SWPD, SWS, and geomagnetic indices across both SC phases. However, CR intensity and SWT exhibit significant phase-dependent discrepancies, with CR fluxes more suppressed during ASC phases, perhaps due to increased solar magnetic complexity and related solar activities. Average parameter values also diverge across storm intensity levels, indicating the modulation role of transient solar phenomena. Correlation coefficient analyses indicate stronger positive and negative associations between CR intensity and solar wind parameters during DSC phases compared to ASC phases, suggesting enhanced coupling between heliospheric conditions and CR flux during the declining solar activity. During weak storms, SWPD and SWT have a minimal influence on CR modulation, whereas their role becomes more pronounced during intense geomagnetic activity. The anomalously subdued solar activity in the ASC phase of SC 24, characterized by lower

*CORRESPONDING AUTHOR:
Chika Onuchukwu, Industrial Physics, Chukwuemeka Odumegwu Ojukwu University, 54 Egbu Road, Uli Campus, Awka 420102, Anambra, Nigeria; Email: onuchukwu71chika@gmail.com

ARTICLE INFO
Received: 24 May 2025 | Revised: 2 August 2025 | Accepted: 18 August 2025 | Published Online: 2 September 2025
DOI: https://doi.org/10.36956/eps.v4i2.2207

CITATION
Onuchukwu, C., Dio, E., 2025. Cosmic Ray Modulation Across Solar Cycles 23 and 24: Phase Dependent Variability and Geomagnetic Storm Effects. Earth and Planetary Science. 4(2): 21–43. DOI: https://doi.org/10.36956/eps.v4i2.2207

SWPD and IMF magnitudes, further emphasizes inter-cycle/phase differences in heliospheric shielding efficiency. These findings highlight the importance of phase- and storm-dependent modulation in space weather forecasting.
Keywords: Cosmic Rays; Geomagnetic Storms; Dst Index; Solar Cycle Phase

1. Introduction

Cosmic rays (CRs), which are high-energy particles originating from galactic, extragalactic, and solar sources, exhibit significant temporal variations as they traverse the heliosphere, modulated by solar activity and the structure of the interplanetary magnetic field (IMF) [1–3]. This modulation is intrinsically linked to the 11-year solar cycle (SC), with galactic cosmic ray (GCR) intensity typically anti-correlated with sunspot numbers (SSNs), a primary indicator of solar activity [4,5]. The relationship between CR flux and solar activity phenomena, however, is not uniform across an entire SC; distinct variations arise during the ascending (ASC) and declining (DSC) phases, driven by differences in solar activities and dynamics [6]. Understanding these statistical patterns is critical not only for advancing solar-terrestrial physics but also for assessing the impact of space weather on satellite operations, aviation, and ground-based technological systems [7,8].

Moreover, CR variations observed at Earth result from modulation processes occurring in both the interplanetary medium and geospace, also influenced primarily by solar activity. In the heliosphere, CRs are modulated by convection with the solar wind, diffusion along and across the IMF, adiabatic energy losses, and drift effects that depend on the solar magnetic polarity [2,9,10]. CMEs and solar flares typically cause shock-induced Forbush Decreases; recurrent Forbush Decreases are associated with corotating interaction regions (CIRs) and high-speed solar wind streams from coronal holes. The persistent nature of these streams and CIRs is what modulates the interplanetary magnetic field, leading to these recurrent drops in CR intensity [11]. Closer to Earth, the geomagnetic field further modulates CRs by imposing a cut-off rigidity, which varies with latitude and geomagnetic conditions [12]. During geomagnetic storms, this shielding weakens, allowing more CRs to penetrate [13]. In the atmosphere, CRs generate secondary particles whose detection is influenced by atmospheric density and seasonal effects [14]. The modulation processes in the heliosphere and geospace are tightly coupled. Changes in solar wind and IMF affect magnetospheric structure and cutoff rigidity, creating a dynamic interaction between interplanetary and geomagnetic conditions [15,16]. This coupling governs the intensity and temporal behavior of cosmic rays reaching Earth.

SCs 23 (1996–2008) and 24 (2008–2019) offer a compelling opportunity for a comparative analysis of CR modulation under distinctly contrasting solar conditions. SC 23 was characterized by relatively high solar activity, evidenced by frequent CME-driven geomagnetic storms. Conversely, SC 24 exhibited anomalous weakness, marked by at least a 30% reduction in sunspot activity, diminished polar magnetic fields, and decreased heliospheric pressure [17,18]. These pronounced solar disparities are directly reflected in CR observations. Generally, GCR intensity exhibits an inverse correlation with solar activity, increasing during the DSC and minimum phases of the SC, and decreasing during the ASC and maximum phases due to enhanced solar modulation [19]. The attenuated heliospheric output observed during SC 24, for example, demonstrably altered CR modulation patterns. This alteration has prompted further inquiry into the evolving protective capacity of the heliosphere against incident CRs [20].

The intricate interplay among CRs and various solar-terrestrial parameters is fundamental to comprehending solar-terrestrial coupling. Key parameters in this context include the interplanetary magnetic field (IMF) magnitude, solar wind speed (SWS), temperature (SWT), and plasma density (SWPD), alongside geomagnetic indices such as Kp, Dst, and ap. These parameters collectively serve as quantitative metrics for characterizing the geoeffectiveness of solar events and the resulting disturbances within Earth's magnetosphere [21,22]. Furthermore, geomagnetic storms, systematically classified by intensity (e.g., strong storm (SS), moderate storm

(MS), weak storm (WS), and non-storm (NS)) based on Dst index thresholds [23], are crucial indicators of space weather activity. The frequency and primary drivers of these storms, such as CMEs and corotating interaction regions (CIRs), exhibit considerable variability both across different SCs and between the ASC and DSC phases of a given cycle [24,25]. Consequently, the variations observed in solar wind parameters and geomagnetic indices across these distinct storm categories provide essential context for understanding the structure and intensity of space weather phenomena [23,26].

While prior studies have established broad correlations between CRs and solar activity [4,27–29], fewer have dissected the interplay of these parameters during specific storm categories across the ASC and DSC phases of SCs 23 and 24. Our analysis in Onuchukwu et al. [30,31], using monthly-averaged data, established that the variability of CR intensity and solar wind parameters demonstrates systematic correlations with SC progression and phase-dependent solar activity patterns. These correlations are attributable to differential heliospheric modulation effects across distinct SCs and their evolutionary phases [2]. Such analyses are vital for refining space weather models, particularly as weaker cycles like SC 24 may indicate fundamental shifts in CR modulation mechanisms or the heliosphere's protective capabilities [15].

This study seeks to investigate (1) CR intensity variations during the ASC and DSC phases of SCs 23 and 24 using daily-averaged observational data; (2) examine statistical correlations between these variations and SSNs, solar wind parameters (IMF, SWS, SWT, and SWPD), and geomagnetic indices (Kp, Dst, ap); and (3) investigate how these relationships diverge across distinct geomagnetic storm classifications (e.g., weak, moderate, strong, and non-storm). By integrating multi-parameter heliospheric and magnetospheric datasets spanning two solar cycles, this work advances the understanding of solar-terrestrial coupling mechanisms and their role in CR modulation under varying solar activity regimes. The findings, we hope, will establish a comparative analytical framework to refine predictive models of space weather dynamics, with emphasis on phase-dependent SC variability and storm-intensity-specific modulation effects.

2. Materials and Methods

The daily average SSN data utilized in this study were obtained from the World Data Center SILSO, Royal Observatory of Belgium, Brussels (http://www.sidc.be/SILSO/). According to SILSO records, SC 23 commenced in August 1996, spanned approximately 12.25 years, reached its maximum in November 2001, and concluded in November 2008. In contrast, SC 24 began in December 2008, attained its maximum in April 2014, and ended in November 2019, with a duration of approximately 11 years.

CR data were acquired from the neutron monitor (NM) station operated by the CR Group of the Geophysical Institute at the National Autonomous University of Mexico (UNAM) (http://www.cosmicrays.unam.mx/). This NM station, located on UNAM's central campus in Mexico City (latitude: 19.330 deg N; longitude: 260.830 deg E; altitude: 2274 m above sea level), has been operational since January 1, 1990, and has an effective vertical cutoff rigidity of 8.2 GV. The present analysis employs daily corrected NM data spanning from 1996 to 2019, thereby encompassing the entirety of SCs 23 and 24. The use of daily averaged CR data is particularly advantageous for reducing the impact of CR diurnal anisotropy, as noted by Dumbovic et al. [32] and Belov et al. [33]. The Mexico NM station offers key advantages for studying the effects of SSN on CR variations due to its moderate cutoff rigidity, low-to-mid geomagnetic latitude, and long-term data availability. Its sensitivity to moderately high-energy CRs makes it ideal for capturing heliospheric modulation effects associated with SSN fluctuations. The station's continuous, high-quality dataset enables robust statistical analysis across multiple solar cycles, supporting the detection of inverse CR-SSN relationships and phase-dependent modulation.

Solar-terrestrial parameters examined include the IMF, in nT, SWS, in km/s, SWT, in K, and SWPD, in N/cm^3. Geomagnetic activity data characterized using the Kp, Dst, and ap indices were also used (the geomagnetic index values used in this study are the cumulative daily averages as presented on the referenced website). All solar wind and geomagnetic data were obtained from the OM-

NIWeb database maintained by NASA's Goddard Space Flight Center (https://omniweb.gsfc.nasa.gov/).

For comparative analysis, each SC was divided into two distinct phases: the ASC and DSC phases. Based on SILSO-defined timings, the ASC phase of SC 23 extended from August 1996 to November 2001, while the DSC phase lasted from December 2001 to November 2008. For SC 24, the ASC phase covered the period from December 2008 to April 2014, and the DSC phase spanned from May 2014 to November 2019. We adopted the two-phase division—comprising the ASC and DSC phases of the solar cycle – in order to emphasize the response of CRs to the temporal gradient of solar activity and to investigate general modulation trends and effects, without the added complexity of solar magnetic polarity considerations. Furthermore, the two-phase approach was favored due to its reduced susceptibility to phase boundary ambiguities, such as the presence of multiple or poorly defined peaks during solar maximum, which could otherwise introduce subjectivity in the segmentation of the data. Within each phase, geomagnetic storm events were further categorized according to their intensity using the Dst index, following established classification schemes[23,34]. The classification is as follows: Strong storms (SS): $-100 \geq \text{Dst} > -150$ nT; Moderate storms (MS): $-50 \geq \text{Dst} > -100$ nT; Weak storms (WS): $-25 \geq \text{Dst} > -50$ nT; Non-storm intervals (NS): > -25 nT. This classification also utilized average daily values of Dst to highlight similarities and differences in the studied parameters across geomagnetic storm categories in different SC phases, enabling a meaningful comparison with the detrended daily SSN averages.

A statistical analysis was carried out to explore the variations and interrelationships among CR intensity, SSNs, solar wind parameters, and geomagnetic indices. Distribution plots were utilized to highlight differences in parameter values during the ASC and DSC phases of both solar cycles. In addition, scatter plots were employed to examine the correlations between CR intensity, solar wind parameters, and geomagnetic indices. Particular attention was given to the correlation between CR flux and SSNs. Previous studies (e.g., Echer et al. (2008), Echer et al. (2011), Usoskin et al. (1998), Usoskin et al. (2001) and Mavromichalaki et al. (2007)[34–38]) have consistently reported a time-lag effect between CR flux and solar activity. In line with these findings, and to focus on the short-term modulation of CRs, our analysis employed daily-averaged CR flux values that were detrended using a 365-day centered moving average. This approach allowed for a clearer interpretation of the dynamic interactions between CR flux and solar-terrestrial parameters during each phase of solar activity.

3. Results and Discussion

3.1. Distribution Plots of CR, SSN, Solar Wind Parameters, and Geomagnetic Indices during the ASC and DSC Phases of SCs 23 and 24

Table 1 presents the statistics of the studied parameters: CR Intensity, SSN, IMF, SWS, SWT, SWPD, and the geomagnetic indices (Kp, Dst, and ap). **Figures 1–3** display the distribution plots using daily average values.

Table 1. Variation of CR with SSN, Solar Wind Parameters, and Geomagnetic Indices During the ASC and DSC Phases of SCs 23 and 24.

	Parameter	Mean	Median	Min	Max	S	K
		ASC	ASC	ASC	ASC	ASC	ASC
SC 23	CR $\times 10^7$	1.8 ± 0.4	1.9	1.2	1.9	-4.5	31.3
SC 24	CR $\times 10^7$	2.1 ± 0.3	2.1	1.3	2.1	-4.9	58.9
SC 23	SSN	109.7 ± 63.1	107.0	0.0	353.0	0.4	-0.5
SC 24	SSN	61.1 ± 42.2	54.0	0.0	220.0	0.5	-0.8
SC 23	IMF (nT)	6.6 ± 2.1	5.9	1.7	32.3	2.3	9.9
SC 24	IMF (nT)	5.1 ± 0.6	4.5	1.6	20.2	1.8	6.0
SC 23	SWT $\times 10^4$ (K)	9.3 ± 5.1	7.5	1.0	67.1	2.2	8.5
SC 24	SWT $\times 10^4$ (K)	7.4 ± 4.2	5.7	1.0	75.1	2.7	14.9
SC 23	SWPD (N/cm^3)	6.8 ± 3.2	5.8	0.5	45.9	1.7	6.3
SC 24	SWPD (N/cm^3)	5.5 ± 2.5	4.8	0.3	33.6	1.6	5.1
SC 23	SWS (km/s)	422.1 ± 65.4	407.0	278.0	829.0	1.1	1.4
SC 24	SWS (km/s)	398.6 ± 63.8	381.0	256.0	744.0	1.1	1.1

Table 1. *Cont.*

	Parameter	Mean	Median	Min	Max	S	K
		ASC	**ASC**	**ASC**	**ASC**	**ASC**	**ASC**
SC 23	Kp	20.5 ± 8.7	20.0	0.0	77.0	0.9	1.0
SC 24	Kp	13.6 ± 7.4	13.0	0.0	57.0	1.1	1.3
SC 23	Dst (nT)	16.1 ± 14.4	-12.0	-211.0	25.0	-2.7	13.4
SC 24	Dst (nT)	9.1 ± 9.6	-7.0	-98.0	19.0	-1.8	5.8
SC 23	ap	12.1 ± 8.2	8.0	0.0	192.0	4.9	38.0
SC 24	ap	6.8 ± 4.5	5.0	0.0	87.0	3.8	23.0
		DSC	**DSC**	**DSC**	**DSC**	**DSC**	**DSC**
SC 23	CR $\times 10^7$	1.9 ± 0.6	1.9	1.3	2.0	-1.1	4.8
SC 24	CR $\times 10^7$	2.1 ± 0.3	2.1	1.8	2.1	-1.0	0.7
SC 23	SSN	61.9 ± 50.7	42.0	0.0	310.0	1.1	0.6
SC 24	SSN	38.3 ± 33.8	24.0	0.0	197.0	1.2	1.0
SC 23	IMF (nT)	6.1 ± 2.1	5.5	1.3	33.4	1.9	8.2
SC 24	IMF (nT)	5.6 ± 1.7	5.0	1.8	21.8	1.8	5.6
SC 23	SWT $\times 10^4$ (K)	11.1 ± 0.6	9.4	0.8	56.1	1.3	2.2
SC 24	SWT $\times 10^4$ (K)	8.9 ± 4.9	7.4	1.0	76.1	2.1	10.0
SC 23	SWPD (N/cm^3)	5.7 ± 2.9	4.6	0.1	42.3	2.0	7.2
SC 24	SWPD (N/cm^3)	6.7 ± 2.9	5.8	0.4	31.8	1.6	3.9
SC 23	SWS (km/s)	461.6 ± 91.4	441.0	257.0	1003.0	0.7	0.1
SC 24	SWS (km/s)	426.4 ± 72.9	405.5	265.0	741.0	0.9	0.2
SC 23	Kp	20.5 ± 9.8	20.0	0.0	77.0	0.7	0.4
SC 24	Kp	17.5 ± 8.3	17.0	0.0	60.0	0.8	0.5
SC 23	Dst (nT)	14.4 ± 12.8	-11.0	-221.0	34.0	-2.8	17.8
SC 24	Dst (nT)	10.6 ± 10.9	-8.0	-127.0	23.0	-1.8	6.7
SC 23	ap	12.0 ± 8.5	8.0	0.0	204.0	5.3	47.1
SC 24	ap	9.5 ± 5.8	6.0	0.0	108.0	3.6	21.8

Note: Mean with standard error; Min is Minimum; Max is Maximum; S is Skewness, and K is Kurtosis of the Distribution.

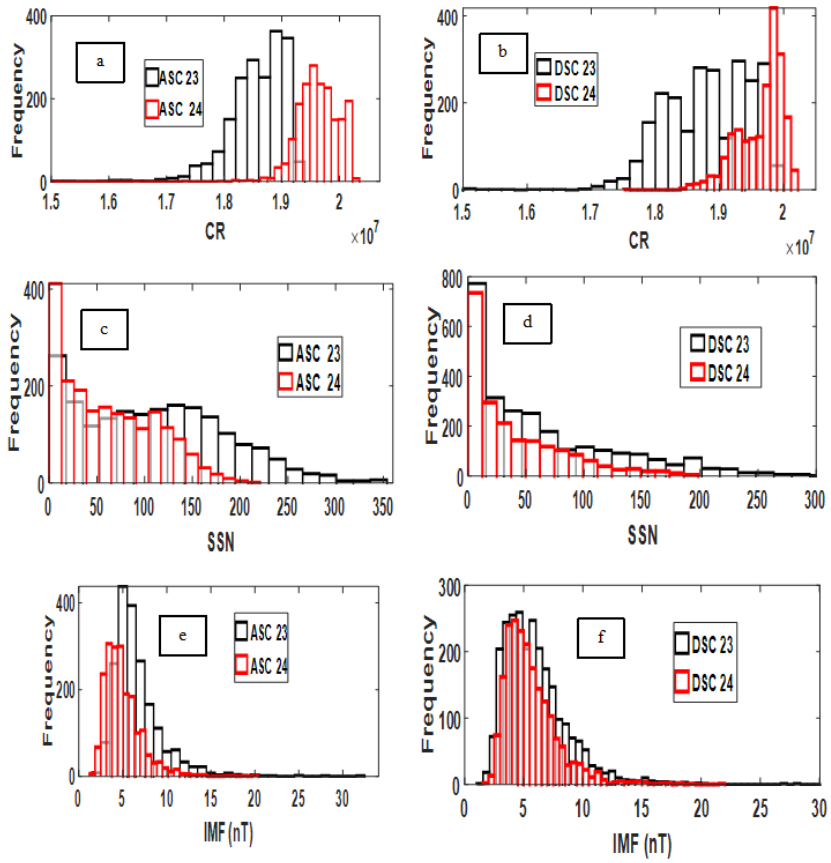

Figure 1. Distribution Plot of Daily-Averaged Values of Cosmic Ray Intensity (**a** and **b**), Sunspot Number (**c** and **d**), and Interplanetary Magnetic Field (**e** and **f**) during the period of 1996–2019, covering the ASC and DSC Phases of Solar Cycles 23 and 24.

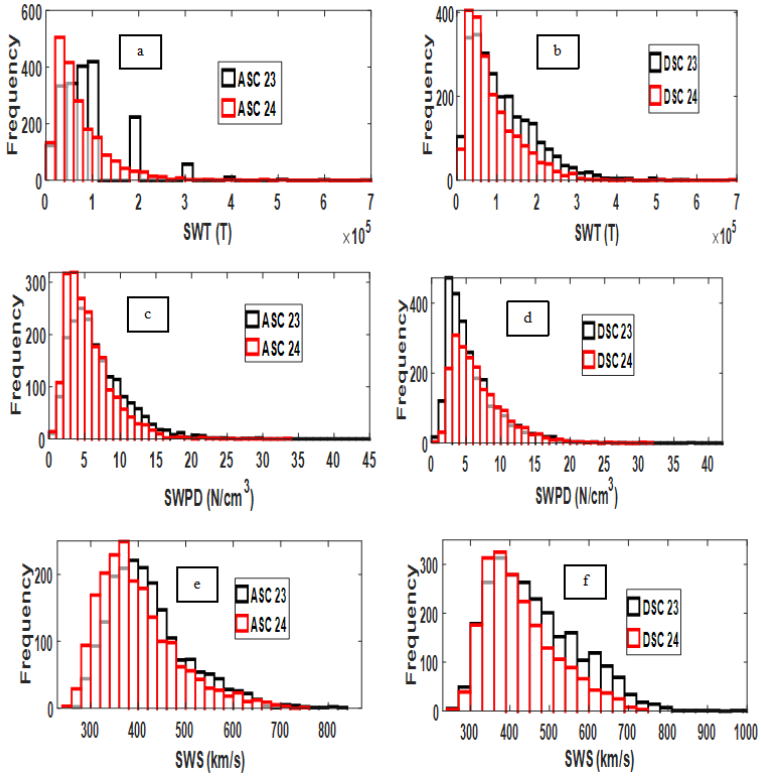

Figure 2. Distribution Plot of Daily-Averaged Values of Solar Wind Temperature (**a** and **b**), Solar Wind Plasma Density (**c** and **d**), and Solar Wind Temperature (**e** and **f**) during the period of 1996–2019 covering the ASC and DSC Phases of Solar Cycles 23 and 24.

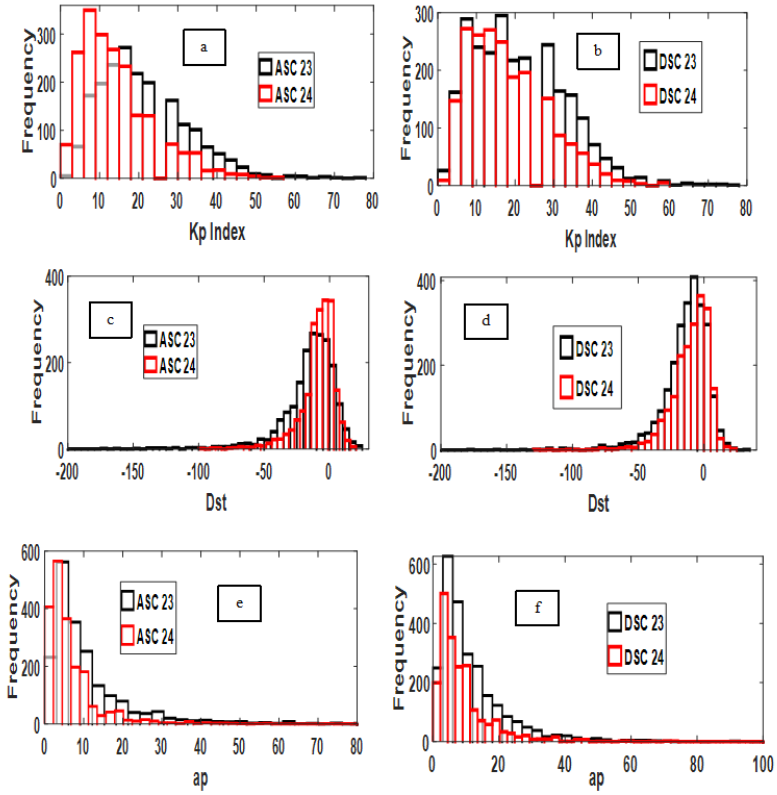

Figure 3. Distribution Plot of Daily-Averaged Values of Kp Index (**a** and **b**), Dst Index (**c** and **d**), and ap Index (**e** and **f**) during the period of 1996–2019 covering the ASC and DSC Phases of Solar Cycles 23 and 24.

The statistical analysis of solar-terrestrial parameters across SCs 23 and 24 during their ASC and DSC phases reveals distinct distributional characteristics driven by varying solar activity levels. From **Table 1**, average CR intensity values appeared lower in SC 23 than in SC 24 (but when you considered the mean values with the standard deviations (SD), they seem to overlap, thus, our discussions will be based on the median values only). **Figure 1** indicates that CR intensity was also lower during ASC phases compared to DSC phases. CR distributions exhibited strong negative skewness and extreme leptokurtosis during ASC phases—SC 23 (S = -4.5; K = 31.3) and SC 24 (S = -4.9; K = 31.3 to 58.9)—pointing to rare, significantly low values linked to heightened solar modulation [2]. In contrast, DSC phases presented reduced skewness and lower kurtosis—SC 23 (S = -1.1; K = 4.8), SC 24 (S = -1.0; K = 0.7)—suggesting a more symmetric, near-normal distribution under diminishing solar activity. Similarly, SSN averages were higher in SC 23 than SC 24 and consistently higher during the ASC than the DSC phases. This is in line with previous findings of stronger solar activity in SC 23 [39–41]. The SSN distribution plots revealed right-skewed behavior in both phases and cycles, particularly during DSC (S = 1.1–1.2; K = 0.6–1.0), reflecting occasional sunspot surges late in the cycle, consistent with the weaker solar activity observed in SC 24 [19].

Solar wind parameters also exhibited marked cycle- and phase-dependent variations. IMF values were higher in the ASC phase of SC 23 but higher during the DSC phase of SC 24. The IMF was characterized by moderate to strong right-skewness (S = 1.8–2.3) and elevated kurtosis (K = 5.6–9.9), indicating sporadic magnetic surges and turbulent enhancements in both cycles. SWT was generally higher during DSC phases (SC 23: 9.2 $\times 10^4$ K; SC 24: 7.4 $\times 10^4$ K) compared to ASC phases (SC 23: 7.5 $\times 10^4$ K; SC 24: 5.7 $\times 10^4$ K), with higher values overall in SC 23. SWPD also showed higher average values during ASC in SC 23 but reversed in SC 24. SC 24 exhibited significantly diminished SSNs, photospheric magnetic field strength, and solar activity. These changes reflect a decline in solar dynamo efficacy and magnetic flux emergence, disrupting coronal heating and reducing open flux, which together lowered SWT and reduced coronal hole activity [42]. During DSC, the Sun's magnetic field simplifies into a dipolar configuration [43], facilitating the formation of high-speed streams (HSS) and corotating interaction regions (CIRs) that elevate plasma temperatures via compression and adiabatic heating [44]. In contrast, the ASC phase is marked by complex closed loops that confine plasma and restrict fast solar wind outflow, leading to cooler, denser solar wind [39]. Positively skewed and leptokurtic distributions of SWT and SWPD, particularly in ASC phases (e.g., SC 24 ASC SWT: S = 2.7, K = 14.9), further support intermittent coronal heating and solar wind bursts during magnetic maxima [45]. SWS was generally faster during DSC phases across both cycles. Its distribution displayed mild skewness (S = 0.7–1.1) and low kurtosis (K = 0.1–1.4), indicating relative stability compared to more volatile parameters like SWT and IMF. We emphasize that while mean values (with associated errors) may suggest no phase-wise differences, distribution plots—along with skewness, kurtosis, and median values—reveal clear distinctions.

The Dst index showed pronounced negative skewness (S = -2.7 to -2.8) and high kurtosis (K = 13.4 to 17.8), especially in SC 23, indicating rare yet severe geomagnetic storms, aligning with prior findings. Similarly, the ap index showed extreme right-skewness (S = 3.6 to 5.3) and high kurtosis (K = 21.8 to 47.1), particularly in SC 23 DSC, pointing to sporadic, intense geomagnetic disturbances driven by strong solar wind-magnetosphere coupling. The Kp index exhibited moderate skewness (S = 0.7–1.1) and low kurtosis, reflecting more regular geomagnetic variability.

Overall, SC 23 displayed more extreme distribution characteristics (i.e., greater skewness and kurtosis) across multiple solar-terrestrial parameters than SC 24, corroborating its higher activity levels [44]. SC 24, with its reduced SSNs and weaker heliospheric dynamics, showed more symmetric, flatter distributions, underscoring a quieter solar environment. These distributional signatures of CRs, solar wind, and geomagnetic indices highlight the importance of solar cycle phase in modulating heliophysical conditions and provide essential input for refining space weather models.

Table 2 synthesizes the statistical characteristics of distribution plots for CR intensity, SSN, solar wind pa-

rameters, and geomagnetic indices derived from daily averaged observational data. While the analysis reveals that these parameters broadly exhibit analogous distributional characteristics across SC phases (e.g., skewness, kurtosis), statistically significant disparities emerge in their central tendency, dispersion, and tail behavior. These differences underscore the nuanced variability in solar-terrestrial coupling mechanisms between ASC and DSC phases, particularly in the magnitude and frequency of extreme values, highlighting phase-dependent modulations in heliospheric and geomagnetic conditions.

The relationship between the correlation coefficient r, the coefficient of determination cc, and the p-values across different phases of SCs reflects the strength, predictability, and statistical significance of associations between CR intensity and various solar/interplanetary parameters and geomagnetic indices, as presented in **Table 3**. While in **Figure 4** shows the scatter plots between CR and SSN, IMF, SWS, SWT, SWPD, and geomagnetic indices (Kp, Dst, ap).

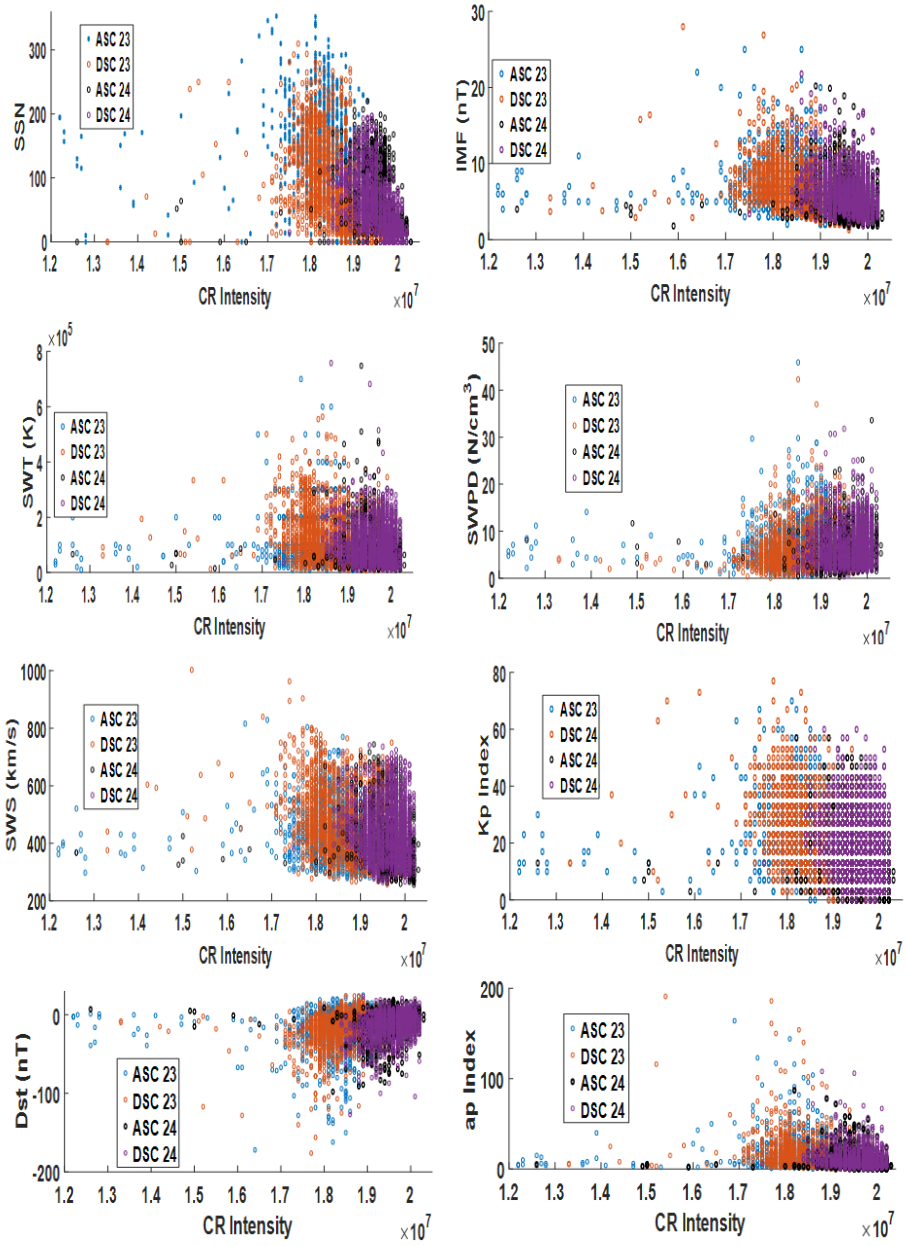

Figure 4. Scatter Plot of CR Intensity against SSN, IMF, SWT, SWPD, SWS, Kp, Dst, and ap using the Daily-Averaged Values from 1996 to 2019 covering the ASC and DSC Phases of Solar Cycles 23 and 24.

Table 2. Summary of the nature of the distribution plots CR, SSN, IMF, SWT, SWPD, SWS, and Geomagnetic Indices (Kp, Dst, ap) during the ASC and DSC Phases of SCs 23 and 24.

Parameter	Phase	Skewness	Kurtosis	Distribution Nature
CR	ASC	Left	Extremely Peaked	Rare deep lows, outliers
	DSC	Mild Left	Mild Peaked	More normal
SSN	ASC/DSC	Right	Near Normal	Moderate to high tail
IMF	ASC/DSC	Right	Peaked	Rare strong bursts
SWT	ASC	Strong Right	Peaked	Solar heating bursts
	DSC	Mild Right	Strong Peaked	Occasional heating
SWPD	ASC/DSC	Right	Peaked	Sporadic plasma density
SWS	ASC/DSC	Mild Right	Near Normal	Smooth distribution
Kp	ASC/DSC	Mild Right	Near Normal	Low disturbance variance
Dst	ASC/DSC	Left	Peaked	Rare strong storms
ap	ASC/DSC	Right	Extremely Peaked	High geomagnetic activity spikes

Table 3. Correlation Coefficient Results Between CR Intensity and the Studied Parameters During the ASC and DSC Phases of SCs 23 and 24. (r is Correlation Coefficient, cc is the Coefficient of Determination, E−x =10^{-x} where x is the exponent).

	ASC 23	ASC 23	ASC 23	DSC 23	DSC 23	DSC 23
Parameters	**r**	**cc**	**p-Value**	**r**	**cc**	**p-Value**
CR/SSN	−0.70	0.49	7.77×10^{-30}	−0.73	0.54	1.16×10^{-30}
CR/IMF	−0.16	0.02	3.88×10^{-10}	−0.45	0.20	2.96×10^{-30}
CR/SWT	−0.18	0.03	1.56×10^{-12}	−0.26	0.07	6.87×10^{-34}
CR/SWPD	0.24	0.06	6.92×10^{-22}	0.04	0.00	8.77×10^{-2}
CR/SWS	−0.25	0.06	2.04×10^{-23}	−0.20	0.04	9.86×10^{-20}
CR/Kp	−0.20	0.04	4.84×10^{-15}	−0.40	0.16	3.31×10^{-30}
CR/Dst	0.06	0.00	1.26×10^{-2}	0.24	0.06	1.46×10^{-28}
CR/ap	−0.15	0.02	1.24×10^{-9}	−0.28	0.08	2.38×10^{-30}
	ASC 24	**ASC 24**	**ASC 24**	**DSC 24**	**DSC 24**	**DSC 24**
CR/SSN	−0.70	0.48	9.79×10^{-30}	−0.75	0.57	1.70×10^{-30}
CR/IMF	−0.20	0.04	1.92×10^{-15}	−0.36	0.13	1.36×10^{-49}
CR/SWT	−0.12	0.01	4.89×10^{-6}	−0.10	0.01	2.52×10^{-5}
CR/SWPD	0.00	0.00	8.99×10^{-1}	−0.04	0.00	7.22×10^{-2}
CR/SWS	−0.13	0.02	1.98×10^{-7}	−0.04	0.00	1.30×10^{-1}
CR/Kp	−0.24	0.06	1.01×10^{-21}	−0.18	0.03	1.39×10^{-13}
CR/Dst	0.15	0.02	2.71×10^{-9}	0.37	0.14	2.07×10^{-30}
CR/ap	−0.19	0.04	7.71×10^{-14}	−0.14	0.02	1.31×10^{-8}

3.2. Correlation Analysis of CR, SSN, Solar Wind Parameters, and Geomagnetic Indices During the ASC and DSC Phases of SCs 23 and 24

During the ASC phase of SC 23 (ASC 23), most correlations between CR intensity and solar parameters are weak ($|r| \leq 0.4$), except for CR and SSN, with a correlation coefficient ~ -0.7. Despite the low correlation and determination coefficients, the associated p-values are extremely small, indicating that most of the observation relationships are nonetheless statistically significant, likely due to the large sample sizes involved. The strongest relationship in this phase is observed between CR and SSN, with r = $-0.7/-0.8$ and cc = 0.5/0.6, suggesting a relatively strong inverse relationship, suggesting that approximately 50–60% of the variation in CR intensity can be explained by SSN fluctuations.

Similarly, during the DSC phase of SC 23 (DSC 23), the correlation remains strong. CR/SSN demonstrates a correlation of r = -0.7, with cc = 0.54 and a highly significant p-value of 1.16×10^{-30}, implying that 54% of CR variability in this phase is attributable to SSN variations. Parameters such as the IMF and geomagnetic index Kp also exhibited stronger correlations relative to the ASC phase. During the DSC of an SC, the Sun's global magnetic field gradually reorganizes into a simpler dipolar configuration, solar activity decreases, and transient events like CMEs become less frequent. As a result, the heliospheric current sheet flattens, and solar wind parameters become more stable[44]; thus, CR solar modulation weakens during the DSC phase[3,16]. A similar trend is evident in the ASC 24. The CR/SSN correla-

tion remains strong (r = -0.7, cc = 0.48), implying that approximately 48% of the CR intensity variation is due to changes in SSN. Although other parameters demonstrate weak correlations with CR, the p-values remain notably low, again reflecting the significance of the results despite relatively low r and cc values. The DSC 24 displays the strongest overall correlations. The CR/SSN pair reaches a peak correlation of r = -0.75, with cc = 0.57 and a p-value of 1.70×10^{-30}, indicating that 57% of CR variability in this phase can be explained by SSN fluctuations. These results are consistent with solar modulation theory, which posits that reduced solar activity during DSC phases permits greater CR penetration into the heliosphere.

Additional observations reveal moderate negative correlations between CR intensity and both the IMF and SWS, particularly during the DSC of SCs 23 and 24. Specifically, CR/IMF correlations were r = –0.45 in DSC 23 and r = -0.36 in DSC 24, while CR/SWS correlations were weaker (r = -0.25 in ASC 23 and r = -0.20 in DSC 23), underscoring the role of heliospheric magnetic structures and solar wind dynamics in modulating CR propagation. Geomagnetic indices also showed inverse relationships with CR intensity. For instance, the CR/Kp correlation was moderately negative during DSC 23 (r = –0.40) and weaker in ASC 23 (r = –0.20), indicating a suppression of CR flux during periods of heightened geomagnetic activity. In contrast, a relatively weak positive correlation was observed between CR intensity and the Dst index during DSC 24 (r = 0.37), suggesting that CR flux tends to increase during geomagnetically quiet intervals. SWPD demonstrated weak or statistically insignificant correlations with CR modulation, except during ASC 23 with r = 0.24 (p = 6.92×10^{-22}), implying a minimal role in influencing CR variability.

These findings are in agreement with established literature on CR modulation. Belov[46] reported statistical evidence supporting the inverse dependence of CR intensity on both solar and geomagnetic activity. Similarly, Richardson[47] reviewed the impact of the solar wind and IMF on energetic particle behavior, including CRs, confirming the moderating effect of heliospheric conditions. Usoskin et al.[4] reconstructed long-term CR modulation patterns across multiple solar cycles, highlighting the inverse relationship between CR intensity and solar activity indices. Dorman[15] further substantiated this by demonstrating significant negative correlations between CRs and parameters such as sunspot number (SSN) and solar wind. Mavromichalaki et al.[48] also confirmed the variability of CRs with SSN, IMF, and solar wind, especially during phases of intensified solar activity. These collective findings reinforce the conclusion that both heliospheric and geomagnetic conditions play critical roles in shaping the temporal evolution of CR flux.

3.3. Phase-Dependent CR Modulation in SCs 23 and 24: Correlating SSNs, Solar Wind Dynamics, and Geomagnetic Indices Across Storm Categories

In **Table 4**, Dst values of -100 to -200 nT were classified as strong storm (SS); Dst values of -50 to -100 nT - moderate storm(MS); Dst values of –25 to –50 nT - weak storm; Dst values of greater –25 nT is non-storm (NS). The severe storms with Dst of -200 nT and less occurred only 4 times in SC 23 and were subsequently not considered in the analysis. The number is the occurrence frequency of each category of storm, while in parentheses, the percentage occurrence. **Table 4** presents the percentage occurrences of geomagnetic activity levels during the ASC and DSC phases of SCs 23 and 24.

Table 4. Frequency of occurrence of each category of geomagnetic storm during the ASC and DSC Phases of SCs 23 and 24.

	SS	MS	WS	NS
ASC 23	17(1%)	89(4%)	337(17%)	1461(74%)
DSC 23	18(1%)	81(3%)	387(16%)	1941(80%)
ASC 24	(0%)	33(2%)	243(12%)	1708(86%)
DSC 24	(0%)	37(2%)	166(9%)	1674(89%)

The percentage values were calculated as

Storm Category% $= \frac{\sum_i^n n_i}{\sum N}$

Where $\sum_i^n n_i$ summation of each storm categories in a phase, and $\sum N$ the total number of storms in each phase.

A noticeable trend is the overall reduction in geomagnetic storm activity from SC 23 to SC 24. In SC 23, strong storms occurred 1% of the time in both phases, while moderate storms occurred at 4% and 3% in the ASC

and DSC phases, respectively. Weak storms accounted for 17% (ASC) and 16% (DSC), while non-storm days made up 74% and 80%. In contrast, during SC 24, strong storms dropped to 0% in both phases, moderate storms reduced to 2% in both, weak storms declined to 12% and 9%, and non-storm days increased significantly to 86% and 89%. This data indicates that SC 24 experienced a significantly quieter geomagnetic environment than SC 23. Furthermore, the DSC phases of both cycles show slightly higher percentages of non-storm days compared to their ASC counterparts, suggesting that geomagnetic activity generally tapers off more during the DSC phase of an SC. The consistent decline in all storm categories, particularly the absence of strong storms in SC 24, supports the established understanding that SC 24 was notably weaker in solar and geomagnetic activity compared to SC 23. This trend aligns with observational studies that describe SC 24 as having fewer and less intense CMEs, which are a primary driver of geomagnetic storms on Earth [35,47]. The prevalence of non-storm days during SC 24 also highlights the reduced risk to technological systems from space weather disturbances during this period.

Table 5 presents a statistical overview of studied parameters - CR intensity, SSN, IMF, SWT, SWPD, SWS, and geomagnetic indices (Kp, Dst, and ap) - during the ASC phases of SCs 23 and 24, across different geomagnetic storm categories, while Table 6 is that of DSC of SCs 23 and 24. These average values are rounded to one decimal place, which may obscure differences in parameter averages across storm categories and solar cycle phases.

Table 5. Statistics of the Parameters Studied During the ASC Phase of SCs 23 and 24 in the different categories of geomagnetic storms (Min is Minimum; Max is Maximum).

	CR	**SSN**	**IMF**	**SWT**	**SWPD**	**SWS**	**Kp**	**Dst**	**ap**
	ASC 23	**ASC 23**	**ASC 23**	**ASC 23**	**ASC 23**	**ASC 23**	**ASC 23**	**ASC 23**	**ASC 23**
	SS	SS	SS	SS	SS	SS	SS	SS	SS
Mean	1.8×10^7	164.5	14.9	1.6×10^5	5.9	608.5	51.2	-120.8	77.2
$SD_{(Mean)}$	3.1×10^5	45.7	3.6	1.1×10^5	3.2	87.1	11.3	12.2	32.3
Median	1.8×10^7	155.0	15.1	1.0×10^5	5.9	630.0	57.0	-118.0	75.0
Max	1.9×10^7	279.0	25.0	6.4×10^5	15.0	770.0	70.0	-102.0	144.0
Min	1.7×10^7	93.0	6.5	1.1×10^4	0.7	401.0	20.0	-150.0	8.0
	MS	MS	MS	MS	MS	MS	MS	MS	MS
Mean	1.8×10^7	146.9	10.1	1.1×10^5	6.7	489.4	38.2	-65.3	36.5
$SD_{(Mean)}$	4.2×10^5	56.1	3.3	6.5×10^4	3.5	76.1	8.8	10.5	15.4
Median	1.8×10^7	148.0	9.3	8.6×10^4	5.3	489.0	40.0	-63.0	32.0
Max	1.9×10^7	346.0	24.5	5.6×10^5	24.1	829.0	63.0	-50.0	164.0
Min	1.6×10^7	0.0	4.1	1.1×10^4	0.7	320.0	3.0	-99.0	2.0
	WS	WS	WS	WS	WS	WS	WS	WS	WS
Mean	1.8×10^7	118.3	7.2	1.3×10^5	5.5	476.4	29.0	-33.5	18.3
$SD_{(Mean)}$	4.6×10^5	66.2	2.1	6.2×10^4	2.6	68.8	7.5	5.4	8.4
Median	1.8×10^7	118.0	6.7	1.1×10^5	4.4	467.0	30.0	-33.0	16.0
Max	1.9×10^7	340.0	17.1	6.7×10^5	27.2	804.0	53.0	-25.0	64.0
Min	1.3×10^7	0.0	3.1	1.0×10^4	1.0	306.0	3.0	-49.0	2.0
	NS	NS	NS	NS	NS	NS	NS	NS	NS
Mean	1.9×10^7	104.6	6.0	8.3×10^4	7.0	403.4	17.1	-7.4	8.2
$SD_{(Mean)}$	4.2×10^5	61.7	1.6	4.3×10^4	3.2	54.8	6.6	5.9	4.2
Median	1.9×10^7	99.0	5.7	6.9×10^4	6.1	393.0	17.0	-8.0	6.0
Max	1.9×10^7	353.0	18.4	4.7×10^5	45.9	721.0	47.0	25.0	53.0
Min	1.2×10^7	0.0	1.7	1.2×10^4	0.5	278.0	0.0	-24.0	0.0
	ASC 24	**ASC 24**	**ASC 24**	**ASC 24**	**ASC 24**	**ASC 24**	**ASC 24**	**ASC 24**	**ASC 24**
	MS	MS	MS	MS	MS	MS	MS	MS	MS
Mean	1.9×10^7	90.9	10.6	1.3×10^5	6.2	477.1	40.1	-64.7	37.2
$SD_{(Mean)}$	2.8×10^5	32.8	2.3	7.7×10^4	2.5	77.6	7.0	9.9	12.8
Median	1.9×10^7	86.0	10.3	9.3×10^4	6.1	467.0	40.0	-62.0	37.0
Max	2.0×10^7	196.0	20.2	5.1×10^5	14.1	668.0	57.0	-50.0	87.0
Min	1.8×10^7	0.0	4.8	2.3×10^4	0.8	339.0	17.0	-98.0	7.0

Table 5. *Cont.*

	CR	SSN	IMF	SWT	SWPD	SWS	Kp	Dst	ap
	ASC 24	**ASC 24**	**ASC 24**	**ASC 24**	**ASC 24**	**ASC 24**	**ASC 24**	**ASC 24**	**ASC 24**
	WS	WS	WS	WS	WS	WS	WS	WS	WS
Mean	1.9×10^7	82.8	6.3	1.3×10^5	4.7	487.0	26.2	−33.4	15.4
$SD_{(Mean)}$	2.4×10^5	29.7	1.8	6.5×10^4	2.5	81.9	7.7	5.5	7.1
Median	1.9×10^7	80.0	5.7	1.2×10^5	3.7	486.0	27.0	−32.5	13.5
Max	2.0×10^7	160.0	19.9	4.8×10^5	22.6	717.0	50.0	−25.0	58.0
Min	1.8×10^7	0.0	2.8	1.3×10^4	0.3	299.0	0.0	−49.0	0.0
	NS	NS	NS	NS	NS	NS	NS	NS	NS
Mean	2.0×10^7	59.7	4.8	6.8×10^4	5.6	389.2	12.0	−5.6	5.4
$SD_{(Mean)}$	2.8×10^5	42.5	1.4	3.7×10^4	2.5	57.1	6.0	6.6	2.9
Median	2.0×10^7	51.0	4.4	5.4×10^4	4.9	375.0	10.0	−5.0	4.0
Max	2.0×10^7	220.0	18.9	7.5×10^5	33.6	744.0	40.0	19.0	42.0
Min	1.3×10^7	0.0	1.7	1.0×10^4	0.6	256.0	0.0	−24.0	0.0

Note: These average values are rounded to one decimal place, which may obscure differences in parameter averages across storm categories and solar cycle phases. Given the overlapping mean values within the standard deviation range, the conclusions drawn here reflect overall trends rather than precise distinctions.

The comparative analysis of SCs 23 and 24 reveals that SC 23 was significantly more geoeffective, exhibiting higher levels of solar and geomagnetic activity, greater variability, and stronger storm-associated parameters. This heightened activity is evident in the mean SSN, which reached 164.5 during strong storm (SS) periods in SC 23, compared to only 90.9 in SC 24, representing an 81% decline in solar activity. Similarly, the IMF averaged 14.9 nT during SS events in SC 23, dropping to 10.6 nT during moderate storms (MS) in SC 24, reflecting a corresponding decline in both the frequency and intensity of CMEs. Solar wind parameters further emphasize this contrast: during SS events, SC 23 experienced faster and hotter solar wind, with average SWS of 608.5 km/s and SWT up to 1.6 $\times 10^5$ K, whereas SC 24 recorded lower averages of 477.1 km/s for SWS and 1.3 $\times 10^5$ K for SWT, indicative of a transition from CME-dominated activity to weaker high-speed streams from coronal holes. Even during non-storm (NS) periods, SC 24 exhibited slower (389.2 km/s vs. 403.4 km/s) and less dense solar wind (5.6 Ncm^{-3} vs. 7.0 Ncm^{-3}), contributing to a generally quieter heliospheric environment.

Geomagnetic indices further underscore the subdued nature of SC 24. During SS periods, the Dst index averaged −120.8 nT in SC 23, nearly double the intensity recorded in SC 24 (−64.7 nT), with similar declines observed in the Kp (from 51.2 to 40.1) and ap indices (from 77.2 to 37.2). Even in weak storm (WS) periods, SC 23 maintained higher levels across SSN, SWS, and SWPD. During NS periods, geomagnetic conditions were notably calmer in SC 24, as reflected by lower average Dst (−5.6 nT vs. −7.4 nT) and Kp (12.0 vs. 17.1) values, suggesting reduced space weather risks to satellites and ground-based systems. This comparative quietude also had implications for CR modulation. The reduced solar activity in SC 24 allowed a greater flux of galactic CRs into the heliosphere, with CR intensity increasing from 1.9 $\times 10^7$ particles in SC 23 to 2.0 $\times 10^7$ during NS periods in SC 24.

Cycle-to-cycle variability also diminished in SC 24, as indicated by lower standard deviations across several parameters. For instance, the standard deviation in SSN during strong storms fell from 54.2 in SC 23 to 41.1 in SC 24, and IMF variability declined from 4.9 nT to 3.1 nT. Similar reductions in the dispersion of solar wind speed, temperature, and geomagnetic indices highlight SC 24 as a more stable but less dynamically impactful cycle. Table 6 provides a comprehensive statistical summary of key space weather parameters—including CR intensity, SSN, IMF, SWT, SWPD, SWS, and geomagnetic indices (Kp, Dst, ap)—during the ASC phases of SCs 23 and 24, across storm categories. Overall, the ASC phase of SC 24 was marked by significantly reduced solar and geomagnetic activity. These findings align with previous studies, e.g., Gopalswamy et al. (2015a), Richardson (2018) [21,49], which attributed the decline in space weather intensity during SC 24 to a broader weakening of heliospheric pressure and magnetic field strength.

Table 6 presents the average values of key heliospheric and geomagnetic parameters during geomagnetic storms in the DSC of SCs 23 and 24. The comparison reveals substantial differences in solar, interplanetary, and geospace conditions, highlighting the broader disparity in

the intensity and structure of the two cycles. SSN trends demonstrate a marked decline in SC 24. During MS, the mean SSN dropped from 106.27 in DSC 23 to 54.91 in DSC 24—a 48% reduction. This pattern persisted during NS intervals, with a decline from 56.03 to 34.97, indicating reduced photospheric magnetic activity in SC 24. CR intensity exhibited an expected inverse relationship with solar activity, consistently higher during DSC 24 across all storm categories. Although SS were absent in DSC 24, CR levels during MS and WS reached 1.93 $\times 10^7$ and 1.94 $\times 10^7$, respectively, both exceeding corresponding DSC 23 values. During NS periods, CR flux increased by ~6%, from 1.89 $\times 10^7$ in DSC 23 to 1.97 $\times 10^7$ in DSC 24, reflecting diminished heliospheric modulation.

Table 6. Statistics of the Parameters Studied During the DSC Phase of SCs 23 and 24 in the different categories of geomagnetic storms.

	CR	**SSN**	**IMF**	**SWT**	**SWPD**	**SWS**	**Kp**	**Dst**	**ap**
	DSC 23	**DSC 23**	**DSC 23**	**DSC 23**	**DSC 23**	**DSC 23**	**DSC 23**	**DSC 23**	**DSC 23**
	SS	SS	SS	SS	SS	SS	SS	SS	SS
Mean	1.8×10^7	129.7	15.7	1.6×10^5	5.6	599.0	59.3	−131.3	112.1
$SD_{(Mean)}$	7.0×10^5	55.1	4.6	1.1×10^5	2.4	124.7	10.3	27.4	45.8
Median	1.8×10^7	107.5	16.1	1.2×10^5	4.4	569.0	63.0	−118.5	112.0
Max	1.9×10^7	250.0	28.0	4.8×10^5	15.1	1003.0	77.0	−100.0	204.0
Min	1.5×10^7	21.0	7.8	1.9×10^4	2.1	388.0	33.0	−221.0	36.0
	MS	MS	MS	MS	MS	MS	MS	MS	MS
Mean	1.8×10^7	106.3	9.3	1.6×10^5	5.3	551.9	39.5	−62.9	36.4
$SD_{(Mean)}$	3.4×10^5	52.2	2.6	8.5×10^4	2.8	96.1	8.7	8.5	16.7
Median	1.8×10^7	94.0	9.2	1.3×10^5	4.3	531.0	40.0	−61.0	33.0
Max	1.9×10^7	247.0	20.3	4.9×10^5	19.6	963.0	63.0	−50.0	102.0
Min	1.7×10^7	15.0	4.1	2.4×10^4	0.1	347.0	3.0	−87.0	2.0
	WS	WS	WS	WS	WS	WS	WS	WS	WS
Mean	1.8×10^7	82.4	7.2	1.8×10^5	4.8	543.0	31.8	−33.3	21.7
$SD_{(Mean)}$	5.2×10^5	52.9	1.9	7.5×10^4	2.3	87.5	7.9	5.7	9.9
Median	1.8×10^7	64.0	6.8	1.7×10^5	4.0	537.0	33.0	−32.0	19.0
Max	2.0×10^7	279.0	18.4	5.6×10^5	21.1	799.0	57.0	−25.0	109.0
Min	1.6×10^7	0.0	2.5	1.3×10^4	0.4	301.0	3.0	−49.0	2.0
	NS	NS	NS	NS	NS	NS	NS	NS	NS
Mean	1.9×10^7	56.0	5.5	9.8×10^4	5.9	439.9	17.1	−7.7	8.3
$SD_{(Mean)}$	5.3×10^5	48.4	1.8	5.4×10^4	2.9	82.3	7.9	5.6	4.8
Median	1.9×10^7	34.0	5.1	8.1×10^4	4.8	419.0	17.0	−8.0	7.0
Max	2.0×10^7	310.0	17.9	4.8×10^5	42.3	801.0	47.0	34.0	54.0
Min	1.3×10^7	0.0	1.3	7.7×10^3	0.4	257.0	0.0	−24.0	0.0
	DSC 24	**DSC 24**	**DSC 24**	**DSC 24**	**DSC 24**	**DSC 24**	**DSC 24**	**DSC 24**	**DSC 24**
	MS	MS	MS	MS	MS	MS	MS	MS	MS
Mean	1.9×10^7	54.9	10.6	1.6×10^5	7.7	515.6	42.5	−64.8	41.4
$SD_{(Mean)}$	2.9×10^5	26.3	3.5	9.1×10^4	4.6	94.9	7.9	9.9	16.4
Median	1.9×10^7	44.0	9.8	1.8×10^5	5.4	532.0	40.0	−61.0	33.0
Max	2.0×10^7	172.0	19.2	6.8×10^5	30.7	741.0	60.0	−50.0	108.0
Min	1.8×10^7	0.0	4.5	2.6×10^4	2.0	356.0	30.0	−100.0	16.0
	WS	WS	WS	WS	WS	WS	WS	WS	WS
Mean	1.9×10^7	59.7	6.9	1.4×10^5	5.5	504.0	29.5	−32.6	18.4
$SD_{(Mean)}$	3.3×10^5	35.6	1.8	5.9×10^4	2.6	79.5	7.4	5.0	8.1
Median	1.9×10^7	55.0	6.5	1.4×10^5	4.4	498.0	30.0	−31.0	16.0
Max	2.0×10^7	181.0	21.8	7.6×10^5	19.7	724.0	50.0	−25.0	60.0
Min	1.8×10^7	0.0	2.7	1.7×10^4	0.4	295.0	3.0	−49.0	2.0
	NS	NS	NS	NS	NS	NS	NS	NS	NS
Mean	2.0×10^7	35.0	5.3	8.0×10^4	6.8	413.4	15.3	−6.3	7.1
$SD_{(Mean)}$	2.6×10^5	32.6	1.5	4.3×10^4	2.9	65.3	6.9	5.4	3.8
Median	2.0×10^7	18.0	4.8	6.4×10^4	5.9	395.0	13.0	−6.0	6.0
Max	2.0×10^7	197.0	18.2	5.2×10^5	31.8	712.0	43.0	23.0	57.0
Min	1.8×10^7	0.0	1.8	1.0×10^4	0.8	265.0	0.0	−24.0	0.0

Note: These average values are rounded to one decimal place, which may obscure differences in parameter averages across storm categories and solar cycle phases. Given the overlapping mean values within the standard deviation range, the conclusions drawn here reflect overall trends rather than precise distinctions.

Solar wind and IMF metrics further differentiate the two cycles. Interestingly, DSC 24 recorded a higher IMF during MS (10.58 nT) than DSC 23 (9.35 nT), likely due to the prevalence of stable, high-speed streams from coronal holes rather than transient CME-driven enhancements. However, IMF values declined slightly during NS periods (5.55 nT to 5.25 nT), consistent with SC 24's overall quiescence. SWS declined systematically in DSC 24. During MS, average SWS fell by 7%, from 551.89 km/s in DSC 23 to 515.58 km/s in DSC 24. NS periods also showed a decrease from 439.87 km/s to 413.43 km/s, indicative of fewer high-speed wind streams. Conversely, SWPD increased in DSC 24. During MS, it averaged 7.73 Ncm^{-3}, compared to 5.29 Ncm^{-3} in DSC 23. A similar trend was noted in NS periods (6.80 vs. 5.92 Ncm^{-3}). SWT trends also reflected this shift. During NS periods, SWT was notably lower in DSC 24 (7.98×10^4 K) compared to DSC 23 (9.83×10^4 K). During WS, SWT declined from 1.78×10^5 K in DSC 23 to 1.44×10^5 K in DSC 24.

Geomagnetic indices (Kp, Dst, ap) underscored the contrast in space weather impact. DSC 23 produced stronger disturbances, with SS storms yielding an average Dst of -131.28 nT and ap of 112.11. These extreme events were absent in DSC 24. However, MS periods in DSC 24 recorded slightly stronger geomagnetic responses—Dst of -64.85 nT vs. -62.90 nT and ap of 41.36 vs. 36.42—possibly due to sustained coronal hole activity. During NS periods, SC 24 remained geomagnetically quieter, with lower Kp (15.25 vs. 17.11) and Dst (-6.28 nT vs. -7.66 nT) than SC 23. Parameter variability also decreased in SC 24. Notably, SSN standard deviation during MS dropped from 60.60 to 35.56, and SWS variability during NS fell from 101.16 to 82.41. In contrast, IMF variability increased slightly during MS in DSC 24 (from 3.27 to 4.03 nT), likely reflecting a more consistent influence from recurrent solar wind sources.

Figures 5–8 are the scatter plots of CR intensity against SSN, IMF, SWT, SWPD, SWS, Kp, Dst and ap using the daily-averaged values for different categories of geomagnetic storm in the period of 1996–2019 covering the ASC and DSC Phases of SCs 23 and 24, while in **Table 7**, we present the correlation coefficient results.

Table 7. Correlation coefficients, the coefficient of determination and the p-values for the relations between CR and SSN, solar parameters (IMF, SWS, SWPD, and SWT), and geomagnetic indices (Kp, Dst, and ap) across the ASC and DSC phases of SCs 23 and 24 during different categories of geomagnetic storms (strong storm [SS], moderate storm [MS], weak storm [WS], non-storm [NS]).

	ASC 23	**ASC 23**	**ASC 23**	**ASC 23**	**DSC 23**	**DSC 23**	**DSC 23**	**ASC 24**	**ASC 24**	**ASC 24**	**DSC 24**	**DSC 24**	**DSC 24**
		r	**cc**	**p**	**r**	**cc**	**p**	**r**	**cc**	**p**	**r**	**cc**	**p**
SS	CR/SSN	−0.2	0.0	0.47	−0.8	0.7	0.00						
SS	CR/IMF	−0.5	0.3	0.02	−0.3	0.1	0.20						
SS	CR/SWT	0.2	0.0	0.54	−0.3	0.1	0.21						
SS	CR/SWPD	0.1	0.0	0.68	0.2	0.0	0.50						
SS	CR/SWS	−0.2	0.1	0.34	−0.4	0.2	0.06						
SS	CR/Kp	−0.4	0.2	0.07	−0.2	0.1	0.33						
SS	CR/Dst	0.1	0.0	0.83	0.3	0.1	0.21						
SS	CR/ap	−0.4	0.1	0.11	−0.4	0.2	0.09						
MS	CR/SSN	−0.5	0.3	0.00	−0.2	0.1	0.03	−0.4	0.2	0.00	−0.2	0.0	0.26
MS	CR/IMF	0.1	0.0	0.33	−0.1	0.0	0.19	0.0	0.0	0.80	0.1	0.0	0.49
MS	CR/SWT	−0.1	0.0	0.66	−0.1	0.0	0.29	−0.1	0.0	0.60	0.1	0.0	0.74
MS	CR/SWPD	0.3	0.1	0.01	0.2	0.0	0.12	0.5	0.3	0.00	−0.1	0.0	0.73
MS	CR/SWS	−0.4	0.1	0.00	−0.4	0.2	0.00	−0.4	0.2	0.00	−0.2	0.0	0.38
MS	CR/Kp	−0.1	0.0	0.25	−0.2	0.0	0.13	−0.1	0.0	0.65	0.0	0.0	0.78
MS	CR/Dst	0.1	0.0	0.24	0.2	0.0	0.05	0.4	0.2	0.00	0.1	0.0	0.53
MS	CR/ap	−0.2	0.0	0.15	−0.1	0.0	0.31	−0.2	0.0	0.19	0.1	0.0	0.77
WS	CR/SSN	−0.3	0.1	0.00	−0.5	0.28	0.00	−0.5	0.2	0.00	−0.6	0.3	0.00
WS	CR/IMF	−0.1	0.0	0.45	−0.3	0.07	0.00	−0.1	0.0	0.13	−0.2	0.0	0.00
WS	CR/SWT	0.0	0.0	0.76	0.0	0.00	0.34	0.0	0.0	0.80	0.1	0.0	0.06
WS	CR/SWPD	0.0	0.0	0.72	0.0	0.00	0.89	0.0	0.0	0.53	0.0	0.0	0.86
WS	CR/SWS	0.0	0.0	0.69	−0.1	0.01	0.13	−0.1	0.0	0.10	0.2	0.1	0.00
WS	CR/Kp	0.0	0.0	0.69	−0.1	0.02	0.01	−0.1	0.0	0.45	0.3	0.1	0.00
WS	CR/Dst	0.0	0.0	1.00	0.2	0.05	0.00	0.2	0.0	0.01	0.2	0.0	0.03
WS	CR/ap	−0.1	0.0	0.55	−0.1	0.02	0.01	−0.1	0.0	0.35	0.3	0.1	0.00

Table 7. *Cont.*

	ASC 23	ASC 23	ASC 23	ASC 23	DSC 23	DSC 23	DSC 23	ASC 24	ASC 24	ASC 24	DSC 24	DSC 24	DSC 24
		r	cc	p	r	cc	p	r	cc	p	r	cc	p
NS	CR/SSN	−0.4	0.1	0.00	−0.6	0.39	0.00	−0.4	0.2	0.00	−0.7	0.4	0.00
NS	CR/IMF	−0.1	0.0	0.00	−0.4	0.18	0.00	−0.1	0.0	0.00	−0.3	0.1	0.00
NS	CR/SWT	−0.1	0.0	0.00	−0.2	0.05	0.00	−0.1	0.0	0.00	−0.1	0.0	0.00
NS	CR/SWPD	0.2	0.0	0.00	0.0	0.00	0.27	0.0	0.0	0.06	0.0	0.0	0.77
NS	CR/SWS	−0.1	0.0	0.00	−0.2	0.03	0.00	−0.1	0.0	0.00	0.0	0.0	0.16
NS	CR/Kp	−0.1	0.0	0.01	−0.3	0.11	0.00	−0.1	0.0	0.00	−0.1	0.0	0.00
NS	CR/Dst	−0.1	0.0	0.04	0.2	0.02	0.00	0.1	0.0	0.00	0.2	0.0	0.00
NS	CR/ap	−0.1	0.0	0.01	−0.3	0.10	0.00	−0.1	0.0	0.00	−0.1	0.0	0.00

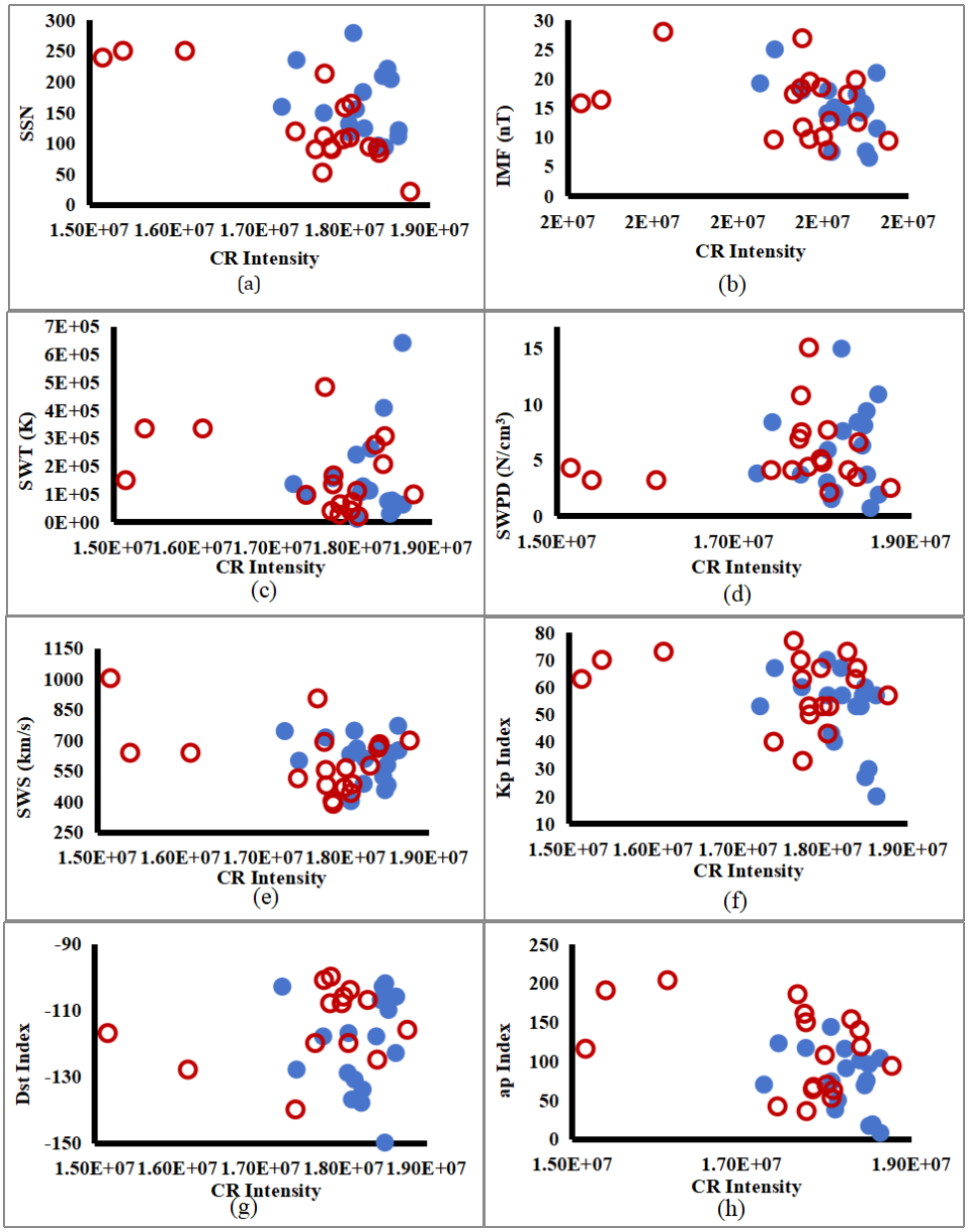

Figure 5. Scatter Plot of CR Intensity against (**a**) SSN, (**b**) IMF (**c**) SWT (**d**) SWPD (**e**) SWS (**f**) Kp (**g**) Dst and (**h**) ap using the Daily-Averaged Values for SS category of Geomagnetic Storm in the period of 1996–2019 covering the ASC and DSC Phases of Solar Cycles 23 and 24 (Legend: Filled Blue Circle- ASC 23; Red Empty Circle - DSC 23).

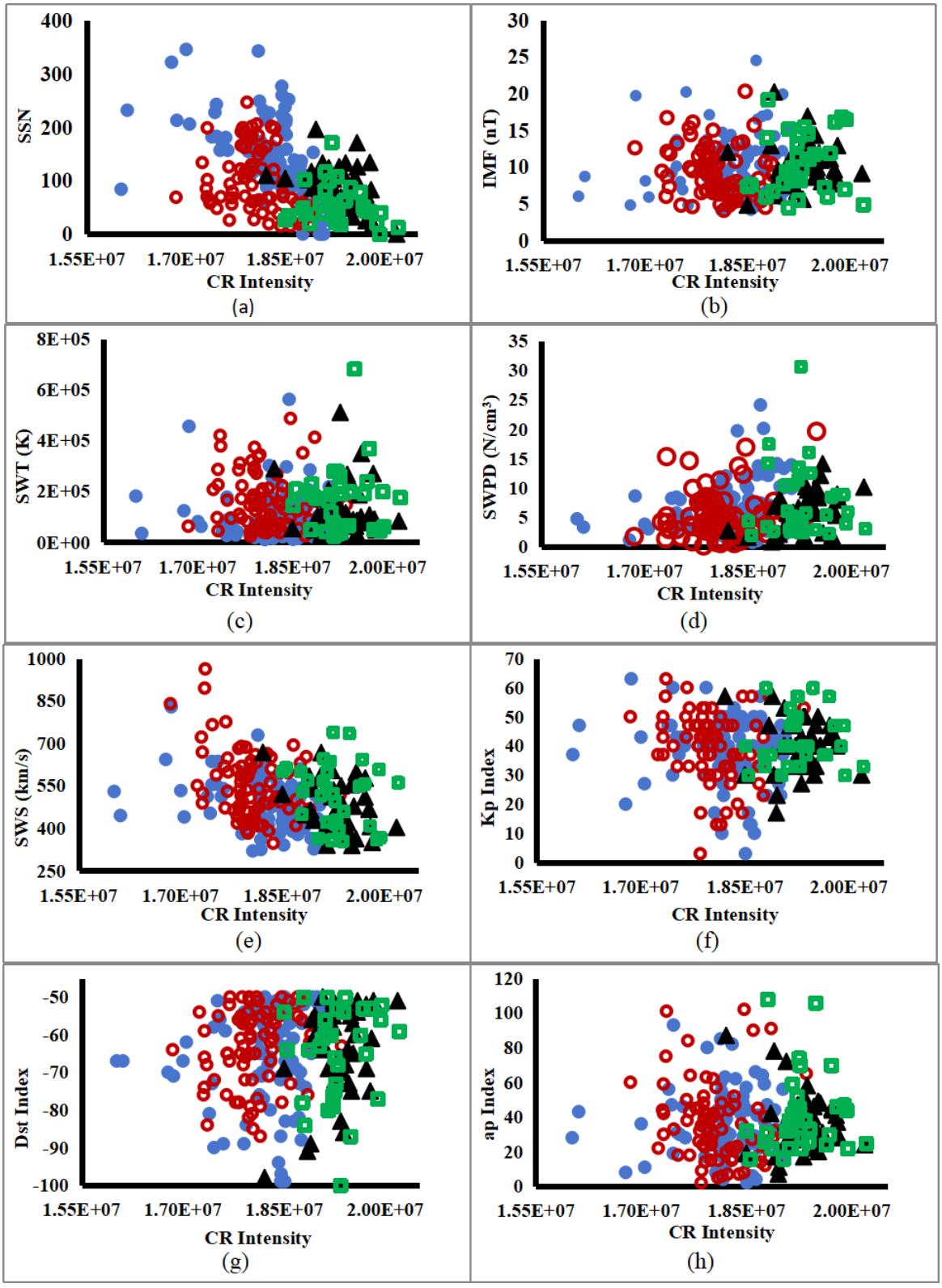

Figure 6. Scatter Plot of CR Intensity against (**a**) SSN, (**b**) IMF (**c**) SWT (**d**) SWPD (**e**) SWS (**f**) Kp (**g**) Dst and (**h**) ap using the Daily-Averaged Values for MS category of Geomagnetic Storm in the period of 1996–2019 covering the ASC and DSC Phases of Solar Cycles 23 and 24 (Legend: Filled Blue Circle – ASC 23; Red Empty Circle – DSC 23; Filled Black Triangle – ASC 24; Green Empty Square – DSC 24).

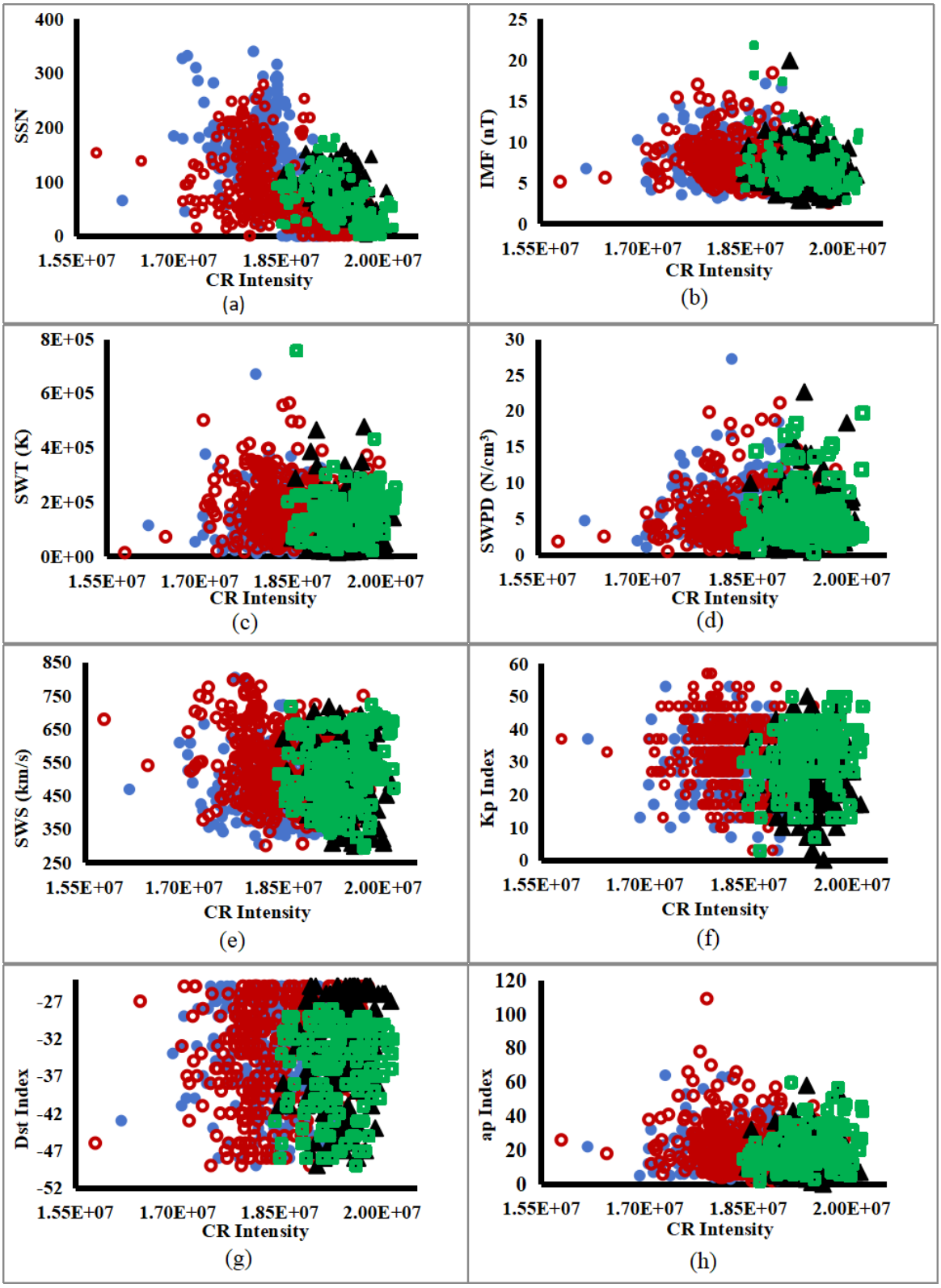

Figure 7. Scatter Plot of CR Intensity against (**a**) SSN, (**b**) IMF (**c**) SWT (**d**) SWPD (**e**) SWS (**f**) Kp (**g**) Dst and (**h**) ap using the Daily-Averaged Values for WS category of Geomagnetic Storm in the period of 1996–2019 covering the ASC and DSC Phases of Solar Cycles 23 and 24 (Legend: Filled Blue Circle – ASC 23; Red Empty Circle – DSC 23; Filled Black Triangle – ASC 24; Green Square – DSC 24).

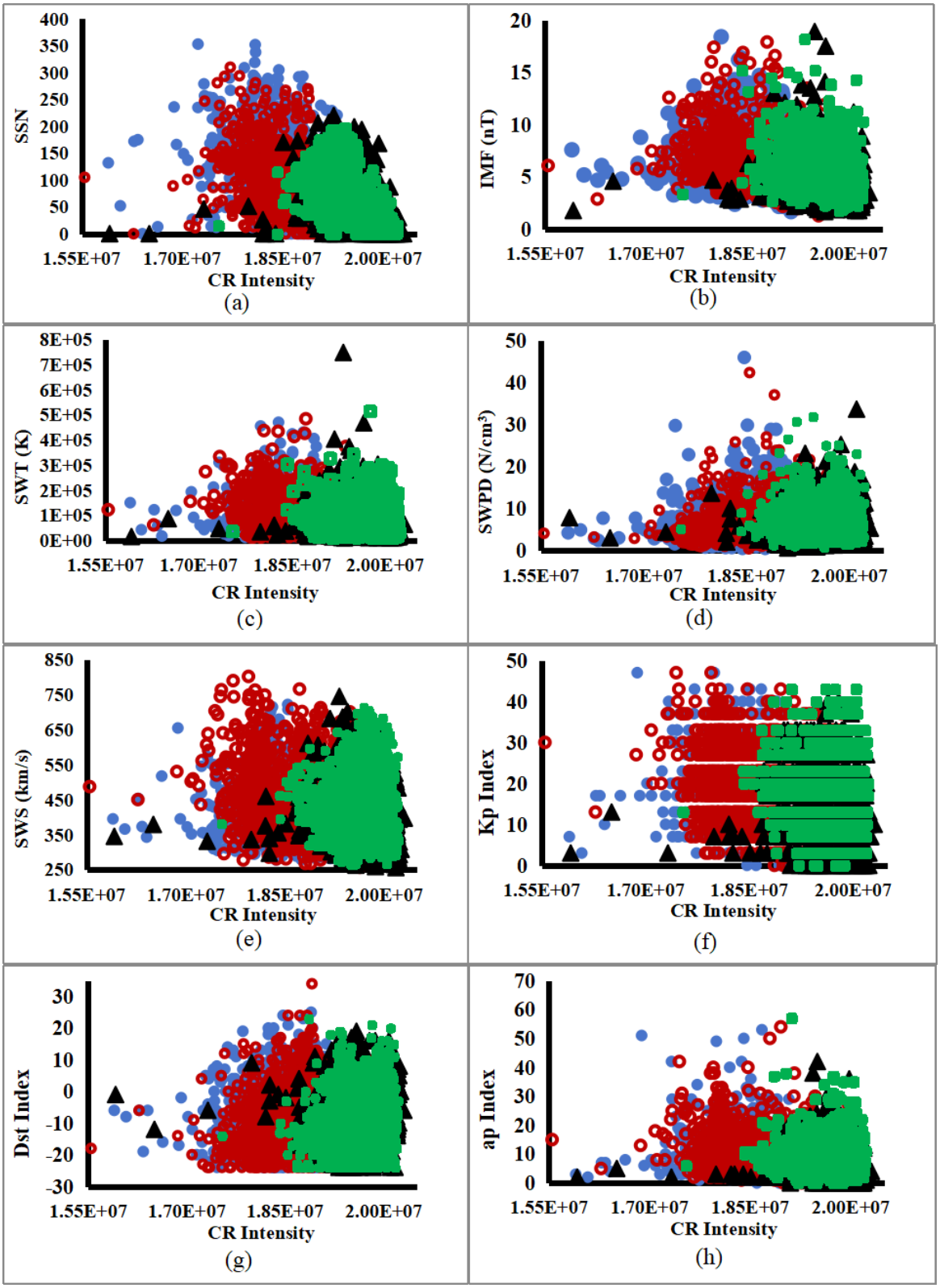

Figure 8. Scatter Plot of CR Intensity against (**a**) SSN, (**b**) IMF (**c**) SWT (**d**) SWPD (**e**) SWS (**f**) Kp (**g**) Dst and (**h**) ap using the Daily-Averaged Values for NS category of Geomagnetic Storm in the period of 1996–2019 covering the ASC and DSC Phases of Solar Cycles 23 and 24 (Legend: Filled Blue Circle – ASC 23; Red Empty Circle – DSC 23; Filled Black Triangle – ASC 24; Green Square – DSC 24).

During the ASC phase of SC 23, CR intensity shows weak to moderate inverse correlations with solar activity parameters. A modest negative correlation is observed with SSN ($r = -0.2$, cc = 0.03, $p \ll 0.05$), while the IMF exhibits a stronger and statistically significant inverse relationship ($r = -0.5$, cc = 0.27, $p = 0.02$), suggesting that enhanced interplanetary magnetic shielding contributes significantly to CR suppression during high solar activity [4,16]. During the descending phase of the SC, the correlation between CR intensity and SSN appears to become stronger ($r = -0.81$, cc = 0.7, $p \ll 0.05$), suggesting an increase modulation process. The increase in correlation could have been driven by the increased prevalence of persistent coronal holes and recurrent high-speed solar wind streams, which were the dominant factors in heliospheric conditions during that phase [50,51]. However, in both the ascending and descending phases, the correlations between CR intensity and geomagnetic indices (Kp, Dst, ap) are generally weak or statistically insignificant. This suggests that solar and interplanetary drivers—rather than geomagnetic responses—play a more direct role in modulating CR intensity during strong magnetic storm.

In MS events during ASC 23, CR intensity demonstrates a moderate and statistically robust inverse correlation with SSN ($r = -0.5$, cc = 0.27, $p \ll 0.05$) and SWS ($r = -0.4$, cc = 0.14, $p \ll 0.05$). These correlations underscore the role of solar wind dynamics in the modulation of CRs, consistent with the theoretical framework proposed by Parker [52] concerning diffusion-dominated cosmic ray transport. In the DSC phase, the significance of SWS persists ($r = -0.4$, $p = 2.0 \times 10^{-4}$), while the CR-SSN correlation weakens ($r = -0.24$, $p = 0.03$), suggesting that the recurrent nature of CIRs dominates CR suppression during this phase over transient sunspot-associated activity [25].

During SC 23, an inverse relationship between CR intensity and SSN was observed in both ASC and DSC phases. However, this correlation was markedly stronger in the DSC phase ($r = -0.53$, cc = 0.28, $p \ll 0.05$) compared to the ASC phase ($r = -0.30$, cc = 0.09, $p \ll 0.05$). This pattern was consistent across both WS and NS conditions, with the DSC-NS phase showing the strongest anti-correlation ($r = -0.63$, cc = 0.39, $p \ll 0.05$) relative to ASC-NS ($r = -0.40$, cc = 0.13, $p \ll 0.05$). These phase-dependent differences are attributed to distinct dominant heliospheric structures. The ASC phase is characterized by transient solar disturbances like CMEs and shocks, which cause irregular CR suppression [47,52]. In contrast, the DSC phase is dominated by long-lived CIRs from recurrent high-speed streams originating from coronal holes. These CIRs provide a more systematic and sustained modulation, enhancing the correlations between CRs and solar activity [53,54]. The robust anti-correlation during the DSC-SS phase ($r = -0.81$) further supports the efficacy of CIRs in modulating CRs, consistent with the global merged interaction region hypothesis [55].

Additional evidence for this phase dependency comes from the stronger DSC-phase correlations between CRs and IMF ($r = -0.43$, $p \ll 0.05$) and solar wind speed (SWS) ($r = -0.17$, $p \ll 0.05$), suggesting efficient modulation by stable heliospheric structures. In contrast, SWT and SWPD showed weak or insignificant correlations across all storm types and phases. For example, SWT exhibited a weak positive correlation during ASC-SS ($r = 0.2$, $p = 0.54$), and SWPD had a modest but significant relationship during MS ($r = 0.3$, $p \ll 0.05$), reflecting their more indirect role in CR diffusion.

Geomagnetic indices (Kp, Dst, ap) generally displayed weak CR correlations, reaffirming the primacy of solar and interplanetary factors. However, they became more relevant during DSC-NS conditions, with CR-Kp ($r = -0.34$, $p \ll 0.05$) and CR-ap ($r = -0.31$, $p \ll 0.05$) showing moderately strong inverse correlations. This suggests that even low-level geomagnetic activity, modulation of CRs may still occur through enhanced magnetospheric turbulence [56].

SC 24 largely follows the same phase-dependent pattern but presents unique characteristics. In the ASC phase, CR intensity shows a moderate inverse correlation with SSN ($r = -0.4$, cc = 0.2, $p \ll 0.05$), consistent with typical solar modulation effects [4]. Notably, SWPD is positively correlated ($r = 0.5$, cc = 0.3, $p < 0.001$), potentially reflecting increased plasma turbulence and CR scattering. A positive correlation with the Dst index ($r = 0.4$, $p \ll 0.05$) suggests that weaker geomagnetic disturbances (less negative Dst) coincide with higher CR in-

tensity. The DSC phase of SC 24, approaching solar minimum, shows a weakening CR-SSN correlation ($r = -0.2$, $p = 0.26$), with SWS and SWPD correlations becoming insignificant ($r = -0.1$ and $r = -0.2$, respectively). Despite this, a strong anti-correlation persists in DSC-NS ($r = -0.7$, cc = 0.44, $p \ll 0.05$), emphasizing the dominant role of solar activity in CR modulation during minima [4]. The IMF maintains a weak but significant inverse correlation in DSC ($r = -0.3$, $p \ll 0.05$)—stronger than in ASC ($r = -0.1$)—consistent with the influence of steady solar wind streams [56]. A unique feature in SC 24 is the shift in SWS correlation, from a marginal inverse relationship in ASC ($r = -0.1$, $p = 0.097$) to a weak positive one in DSC ($r = 0.2$, $p \ll 0.05$).

This anomaly, not observed in SC 23, may reflect altered solar wind structures or a weaker magnetic field, allowing intermittent CIRs to enhance CR penetration [50]. Unexpectedly, CRs also show a positive correlation with Kp and ap indices in DSC-WS ($r = 0.3$, $p \ll 0.05$ for both), which may be a result of localized magnetospheric compression or solar wind discontinuities coinciding with CR enhancements [56].

Overall, CR intensity variations are predominantly governed by solar and interplanetary parameters, with SSN and SWS serving as the most influential modulators, especially during the DSC phase. The ASC phase is characterized by transient modulation from CMEs, while the DSC phase is dominated by the sustained influence of recurrent CIRs [16]. The emergence of phase- and cycle-specific anomalies, such as the unique positive CR-SWS correlation in SC 24, underscores the need for refined, cycle-specific models to improve our understanding of heliospheric dynamics and space weather forecasting.

4. Conclusions

This study presents a statistical investigation into the variability of CR intensity across the ASC and DSC phases of SCs 23 and 24, with a specific focus on different categories of geomagnetic storms. Utilizing distribution plots and correlation analyses, we examined the behavior of several solar and heliospheric parameters, including SSN, IMF, SWPD, SWS, SWT, and geomagnetic indices, in relation to CR intensity.

Our findings indicate that the distributions of SSN, IMF, SWPD, SWS, and geomagnetic indices generally exhibit similar trends across both ASC and DSC phases of SC 23 and 24. However, CR intensity and SWT show noticeable phase-dependent deviations. Moreover, the average values of these parameters seem to vary across SC phases and storm intensity categories. Our results indicate that the modulation of CRs during SCs 23 and 24 is strongly influenced by heliospheric conditions, including sunspot activity and the IMF. The observed differences between the ASC and DSC phases are attributable to phase-specific solar dynamics. During ASC phases, intensified solar activity will result in frequent CMEs, increased heliospheric current sheet tilt, and these will generate a more disturbed and turbulent heliosphere that enhances CR modulation (see e.g., Potgieter et al. (2013), Heber et al. (2009), Wiedenbeck et al. (2005) [57–59]). Also, elevated solar wind speed and density during this phase further amplify modulation effects (e.g., Mathpal et al. (2018) [60]). Additionally, variations in solar magnetic field behavior and meridional flow between SCs 23 and 24 [61,62] will likely contribute to the contrasting CR–solar wind–geomagnetic relationships observed across the two cycles and their phases.

Correlation coefficient results (**Tables 3** and **7**) generally reveal stronger correlations - either positive or negative - during the DSC phases compared to the ASC phases, suggesting enhanced coupling between the studied parameters and CR modulation during the DSC phases. Our correlation analysis results indicate that the dominant drivers of CR modulation across both cycles are SSN, and IMF strength. While SSN is not the direct cause CR suppression, its strong inverse correlation with CR intensity ($r \approx -0.70$) to -0.75) highlights its role as an indicator of solar activity. Higher SSN values correspond to an increase in solar events like CMEs, which are the direct cause of the suppression of CR flux. IMF exhibits a moderate negative correlation, especially during DSC phases ($r = -0.36$ to -0.45), underscoring the shielding effect of enhanced heliospheric magnetic fields. Geomagnetic indices also display moderate negative correlations, more pronounced in DSC phases. SWS shows a weaker but notable inverse correlation, mainly in ASC phases, while SWT and SWPD have weak and inconsis-

tent relationships with CRs. Interestingly, the Dst index shows a positive correlation with CR, particularly during DSC phases, indicating an indirect link through geomagnetic storm strength. Overall, SSN and IMF, emerge as the most influential factors in GCR modulation, with stronger effects observed during descending phases.

Author Contributions

C.O. conceived and wrote the article, while E.D. revised and improved it. All authors have read and agreed to the published version of the manuscript.

Funding

This work received no external funding.

Institutional Review Board Statement

Not Applicable.

Informed Consent Statement

Not Applicable.

Data Availability Statement

Sunspot data (http://www.sidc.be/SILSO); National Autonomous University of Mexico (UNAM) (http://www.cosmicrays.unam.mx/) cosmic ray data; solar wind parameters (https://omniweb.gsfc.nasa.gov/).

Conflicts of Interest

The authors declare no conflict of interest.

Abbreviation

Below is the list of parameters used in this study:

CR	Cosmic Ray intensity recorded at neutron station on Earth
SSN	Sunspot number
IMF	Interplanetary Magnetic Field
SWPD	Solar Wind Plasma Density
SWT	Solar Wind Temperature
SWS	Solar Wind Speed
Kp	Kennziffer planetary index quantifies disturbances in the Earth's geomagnetic field over 3-hour intervals, due to solar wind and interplanetary magnetic field (IMF) fluctuations
Dst	Disturbance Storm Time index is a global geomagnetic index that measures the intensity of the ring current in Earth's magnetosphere, which intensifies during geomagnetic storms
ap	Amplitude planetary index is daily measure of geomagnetic activity on Earth

References

[1] Parker, E.N., 1958. Dynamics of the interplanetary gas and magnetic fields. Astrophysical Journal. 128, 664. DOI: https://doi.org/10.1086/146579

[2] Potgieter, M.S., 2013. Cosmic Rays in the Inner Heliosphere: Insights from Observations, Theory and Models. Space Science Reviews. 176(1), 165–176. DOI: https://doi.org/10.1007/s11214-011-9750-7

[3] Lockwood, M., Owens, M.J., Barnard, L., et al., 2016. Tests of Sunspot Number Sequences: 2. Using Geomagnetic and Auroral Data. Solar Physics. 291, 2811–2828.

[4] Forbush, S.E., 1954. World-wide cosmic ray variations, 1937–1952. Journal of Geophysical Research. 59, 525–542. DOI: https://doi.org/10.1029/JZ059i004p00525

[5] Bazilevskaya, G.A., Usoskin, I.G., Flückiger, E.O., et al., 2008. Cosmic ray induced ion production in the atmosphere. Space Science Reviews. 137(1–4), 149–173.

[6] Hathaway, D.H., 2010. The solar cycle. Living Reviews in Solar Physics. 7(1), 1.

[7] Vainio, R., Desorgher, L., Heynderickx, D., et al., 2009. Dynamics of the Earth's particle radiation environment. Space Science Reviews. 147, 187–231.

[8] Schwadron, N.A., Spence, H.E., Jordan, A.P., et al., 2014. Does the worsening galactic cosmic radiation environment observed by CRaTER preclude future manned deep space exploration? Space Weather. 12(11), 622–632.

[9] Jokipii, J.R., 1971. Propagation of cosmic rays in the solar wind. Reviews of Geophysics. 9(1), 27–87.

[10] Burger, R.A., Potgieter, M.S., 1989. The effect of large-scale drift and the heliospheric current sheet on cosmic-ray modulation. The Astrophysical Jour-

nal. 339, 501–511.

[11] Cane, H.V., 2000. Coronal mass ejections and Forbush decreases. Space Science Reviews. 93(1–2), 55–77.

[12] Smart, D.F., Shea, M.A., 2003. The local time asymmetry of geomagnetic cutoff rigidities. Advances in Space Research. 31(4), 809–814.

[13] Kudela, K., Usoskin, I.G., 2004. On magnetospheric transmissivity of cosmic rays. Czechoslovak Journal of Physics. 54(2), 239–254.

[14] Dorman, L.I., 2004. Cosmic Rays in the Earth's Atmosphere and Underground. Springer: Berlin, Germany.

[15] Richardson, I.G., Cane, H.V., 2011. Galactic cosmic ray intensity response to interplanetary coronal mass ejections/magnetic clouds in 1995–2009. Solar Physics. 270, 609–627.

[16] Usoskin, I.G., Kovaltsov, G.A., Shea, M.A., 2008. Long-term geomagnetic indices and cosmic ray modulation. Advances in Space Research. 42(7), 1304–1310.

[17] Nandy, D., Muñoz-Jaramillo, A., Martens, P.C.H., 2011. The unusual minimum of sunspot cycle 23 caused by meridional plasma flow variations. Nature. 471(7336), 80–82.

[18] Pesnell, W.D., 2016. Predictions of solar cycle 24: How are we doing? Space Weather. 14(1), 10–21.

[19] Aslam, O.P.M., Badruddin, 2012. Influence of solar and interplanetary parameters on cosmic-ray intensity during different solar activity conditions. Solar Physics. 279(2), 269–290.

[20] Gopalswamy, N., Yashiro, S., Akiyama, S., et al., 2015b. Properties and geoeffectiveness of magnetic clouds during solar cycles 23 and 24. Journal of Geophysical Research: Space Physics. 120(11), 9221–9245.

[21] Gopalswamy, N., Yashiro, S., Michalek, G., et al., 2015a. A catalog of halo coronal mass ejections from Solar Cycle 23. Journal of Geophysical Research: Space Physics. 120(9), 7351–7366.

[22] Richardson, I.G., Cane, H.V., 2012. Near-Earth interplanetary coronal mass ejections during solar cycle 23 (1996–2009): Catalog and summary of properties. Solar Physics. 264(1), 189–237.

[23] Gonzalez, W.D., Joselyn, J.A., Kamide, Y., et al., 1994. What is a geomagnetic storm? Journal of Geophysical Research: Space Physics. 99(A4), 5771–5792.

[24] Tsurutani, B.T., Gonzalez, W.D., Gonzalez, A.L.C., et al., 2006. Interplanetary origin of geomagnetic activity in the declining phase of the solar cycle. Journal of Geophysical Research: Space Physics. 100(A11), 21717–21733.

[25] Kilpua, E.K.J., Balogh, A., von Steiger, R., et al., 2017. Geoeffective properties of solar transients and stream interaction regions. Space Science Reviews. 212, 1271–1314.

[26] Zhang, X., Wang, Y., He, W., et al., 2020. Statistical study of cosmic ray modulation and solar wind properties during solar cycles 23 and 24. Solar Physics. 295(6), 79.

[27] Tomassetti, N., Bertucci, B., Fiandrini, E., 2022. New insights from cross-correlation studies between Solar activity and Cosmic-ray fluxes. Proceedings of Science (ICRC2021). 1324, 1253.

[28] Miyake, S., Asaoka, Y., Ave, M., et al., 2023. Cosmic-Ray Modulation during Solar Cycles 24-25 Transition Observed with CALET on the International Space Station. Proceedings of Science. 444, 1253.

[29] Singh, S., 2023. Cosmic-Ray Modulation in relation to Solar and Heliospheric Parameters. Proceedings of the 38th International Cosmic Ray Conference (ICRC2023); Nagoya, Japan; 26 July–3 August 2023.

[30] Onuchukwu, C.C., Dio, E., Leghara, E., 2024. Asian Basic and Applied Research Journal. 6(1), 192–224.

[31] Onuchukwu, C.C., Dio, E., Onyebueke, E.O., 2025. Asian Basic and Applied Research Journal. 7(1), 145–168.

[32] Dumbović, M., Vršnak, B., Calogovic, J., et al., 2011. Astronomy and Astrophysics. 531(A91), 1.

[33] Belov, A., Eroshenko, E., Yanke, V., et al., 2018. The global survey method applied to ground-level cosmic ray measurements. Solar Physics. 293(4), 68. DOI: https://doi.org/10.1007/s11207-018-1277-6

[34] Echer, E., Gonzaleza, W.D., Tsurutani, B.T., 2011. Statistical studies of geomagnetic storms with peak Dstr 50 nT from 1957 to 2008. Journal of Atmospheric and Solar-Terrestrial Physics. 73, 1454–1459.

[35] Echer, E., Gonzalez, W.D., Tsurutani, B.T., et al., 2008. Interplanetary conditions causing intense geomagnetic storms (Dst ≤ -100 nT) during solar cycle 23 (1996–2006). Journal of Geophysical Research: Space Physics. 113(A5). DOI: https://doi.org/10.1029/2007JA012744

[36] Usoskin, I.G., Alanko, K., Mursula, K., et al., 1998. Heliospheric modulation of cosmic rays: Monthly reconstruction for 1951–2004. Journal of Geophysical Research: Space Physics. 103(A6), 9567–9574.

[37] Usoskin, I.G., Mursula, K., Kovaltsov, G.A., 2001. Heliospheric modulation of cosmic rays and solar activity during the Maunder minimum. Journal of Geophysical Research: Space Physics. 106(A8), 16039–16046.

[38] Mavromichalaki, H., Paouris, E., Petropoulos, B., 2007. The relationship of galactic cosmic rays to the sunspot number. Annales Geophysicae. 25(1), 185–188.

[39] Shen, Z., Qin, G., Zuo, P., et al., 2020. A study of variation of GCR intensity based on a hybrid data processing method. The Astrophysical Journal. 900(2), 143.

[40] Kane, R.P., 2002. Some implications using the group sunspot number reconstruction. Solar Physics. 205 (2), 383–401. DOI: https://doi.org/10.1023/A:1014296529097

[41] Javaraiah, J., 2016. North-south asymmetry in small and large sunspot group activity and violation of even-odd solar cycle rule. Astrophysics and Space Science. 361(7), 208.

[42] Dagnew, F.K., Gopalswamy, N., Tessema, S.B., et al., 2020. Intercycle and intracycle variation of halo CME rate obtained from SOHO/LASCO observations. The Astrophysical Journal. 903(2), 118.

[43] Schrijver, C.J., Livingston, W.C., Woods, T.N., et al., 2011. The minimal solar activity in 2008–2009 and its implications for long-term climate modeling. Geophysical Research Letters. 38(6). DOI: https://doi.org/10.1029/2011GL046658

[44] Abramenko, V.I., Yurchyshyn, V.B., Watanabe, H., 2010. Relationship between coronal hole parameters and solar wind high-speed streams. Solar Physics. 262(2), 199–212.

[45] McComas, D.J., Alexashov, D., Bzowski, M., et al., 2013. The heliosphere's interstellar interaction: No bow shock. Science. 336(6085), 1291–1293.

[46] Belov, A., 2000. Large Scale Modulation: View From the Earth. Space Science Reviews. 93, 79–105.

[47] Richardson, I.G., 2004. Energetic particles and corotating interaction regions in the solar wind. Space Science Reviews. 111(3–4), 267–376.

[48] Mavromichalaki, H., Papaioannou, A., Plainaki, C., et al., 2011. Space weather effects on cosmic rays. Advances in Space Research. 47(12), 2210–2222.

[49] Richardson, I.G., 2018. Solar wind stream interaction regions throughout the heliosphere. Living Reviews in Solar Physics. 15(1), 1–98. DOI: https://doi.org/10.1007/s41116-017-0011-z

[50] Moraal, H., Stoker, P., 2010. The modulation of cosmic rays during the last solar minimum. Advances in Space Research. 46(9), 1184–1188.

[51] Richardson, J.D., Paularena, K.I., Belcher, J.W., et al., 1999. The Solar Wind During the Solar Cycle: Ulysses and Voyager 2 Observations. Journal of Geophysical Research: Space Physics. 104(A8), 17249–17261.

[52] Cliver, E.W., Ling, W.T., 2001. 22 Year Patterns in the Relationship of Sunspot Number and Tilt Angle to Cosmic-Ray Intensity. The Astrophysical Journal. 551(2), L189–L192.

[53] Dalla, S., Lario, S., Richardson, I.G., 2015. Galactic cosmic ray intensity depressions and recurrent magnetic structures. Journal of Geophysical Research: Space Physics. 120(1), 3–17.

[54] Badruddin, S., Singh, M., Dabas, V.D., 2008. Cosmic ray variations during solar cycle 23. Journal of Atmospheric and Solar-Terrestrial Physics. 70(14), 1827–1836.

[55] Cane, H.V., Richardson, I.G., von Rosenvinge, T.T., 1999. Cosmic ray decreases and solar wind disturbances during the 1979–1986 solar minimum. Journal of Geophysical Research: Space Physics. 104(A12), 28249–28260.

[56] Dumbović, M., Heber, B., Vršnak, B., et al., 2018. Statistical relation between solar proton events and associated coronal mass ejections and solar flares. Solar Physics. 293(8), 112.

[57] Potgieter, M.S., 2013. Solar Modulation of Cosmic Rays. Living Reviews in Solar Physics. 10(1), 3.

[58] Heber, B., Kopp, A., Gieseler, J., et al., 2009. Modulation of Galactic Cosmic Ray Protons and Electrons During an Unusual Solar Minimum. The Astrophysical Journal. 699(2), 1956–1963.

[59] Wiedenbeck, M.E., Davis, A.J., Leske, R.A., et al. The Level of Solar Modulation of Galactic Cosmic Rays from 1997 to 2005 as Derived from ACE Measurements of Elemental Energy Spectra. In Proceedings of the 29th International Cosmic Ray Conference, Pune, India, 3–10 August 2005; pp. 277.

[60] Mathpal, C., Prasad, L., Pokharia, M., et al., 2018. Study of cosmic ray intensity in relation to the interplanetary magnetic field and geomagnetic storms for solar cycle 24. Astrophysics and Space Science. 363(8), 177. DOI: https://doi.org/10.1007/s10509-018-3390-2

[61] Hathaway, D.H., Rightmire, L., 2010. Variations in the Sun's Meridional Flow over a Solar Cycle. Science. 327(5971), 1350–1352.

[62] Upton, L., Hathaway, D.H., Sushant, M. Variations in the Suns Axisymmetric Flows During Solar Cycles 23 and 24. In AGU Fall Meeting, New Orleans, LA, USA, 13–17 December 2021.